2011

Lyapunov-based Control Design For Uncertain Mimo Systems

Zhao Wang
University of Central Florida

Lyapunov-Based Control Design for Uncertain MIMO Systems

by

Zhao Wang
B.E. Zhejiang University, 2008
M.S.E.E University of Central Florida, 2011

A dissertation submitted in partial fulfillment of the requirements
for the degree of Doctor of Philosophy
in the Department of Electrical Engineering and Computer Science
in the College of Engineering and Computer Science
at the University of Central Florida
Orlando, Florida

Fall Term
2011

Major Professor: Aman Behal

ABSTRACT

In this dissertation. we document the progress in the control design for a class of MIMO nonlinear uncertain system from five papers. In the first part, we address the problem of adaptive control design for a class of multi-input multi-output (MIMO) nonlinear systems. A Lypaunov based singularity free control law, which compensates for parametric uncertainty in both the drift vector and the input gain matrix, is proposed under the mild assumption that the signs of the leading minors of the control input gain matrix are known. Lyapunov analysis shows global uniform ultimate boundedness (GUUB) result for the tracking error under full state feedback (FSFB). Under the restriction that only the output vector is available for measurement, an output feedback (OFB) controller is designed based on a standard high gain observer (HGO) stability under OFB is fostered by the uniformity of the FSFB solution. Simulation results for both FSFB and OFB controllers demonstrate the efcacy of the MIMO control design in the classical 2-DOF robot manipulator model.

In the second part, an adaptive feedback control is designed for a class of MIMO nonlinear systems containing parametric uncertainty in both the drift vector and the input gain matrix, which is assumed to be full-rank and non-symmetric in general. Based on an SDU decomposition of the gain matrix, a singularity-free adaptive tracking control law is proposed that is shown to be globally asymptotically stable (GAS) under full-state feedback.

Output feedback results are facilitated via the use of a high-gain observer (HGO). Under output feedback control, ultimate boundedness of the error signals is obtained the size of the bound is related to the size of the uncertainty in the parameters. An explicit upper bound is also provided on the size of the HGO gain constant.

In third part, a class of aeroelastic systems with an unmodeled nonlinearity and external disturbance is considered. By using leading- and trailing-edge control surface actuations, a full-state feedforward/feedback controller is designed to suppress the aeroelastic vibrations of a nonlinear wing section subject to external disturbance. The full-state feedback control yields a uniformly ultimately bounded result for two-axis vibration suppression. With the restriction that only pitching and plunging displacements are measurable while their rates are not, a high-gain observer is used to modify the full-state feedback control design to an output feedback design. Simulation results demonstrate the ef cacy of the multi-input multi-output control toward suppressing aeroelastic vibration and limit cycle oscillations occurring in pre and post utter velocity regimes when the system is subjected to a variety of external disturbance signals. Comparisons are drawn with a previously designed adaptive multi-input multi-output controller.

In the fourth part, a continuous robust feedback control is designed for a class of high-order multi-input multi-output (MIMO) nonlinear systems with two degrees of freedom containing unstructured nonlinear uncertainties in the drift vector and parametric uncertainties in the high frequency gain matrix, which is allowed to be non-symmetric in general. Given some mild assumptions on the system model, a singularity-free continuous robust tracking con-

trol law is designed that is shown to be semi-globally asymptotically stable under full-state feedback through a Lyapunov stability analysis. The performance of the proposed algorithm have been verified on a two-link robot manipulator model and 2-DOF aeroelastic model.

To my parents and my wife

ACKNOWLEDGMENTS

First of all, I would like to express my gratitude to my advisor, Dr. Aman Behal, for his insightful guidance that is so helpful to the work I have conducted in University of Central Florida. He is incessantly encouraging, supportive, and ready to provide practical help and advice, from basic theoretical details to higher level research.

I am also grateful to my committee members: Dr. Piergiovanni Marzocca, Dr. Ladislau Boloni, Dr. Michael Haralambous, for inspiring discussions on my research.

I would like to thank Dr. Dae-Jin Kim, Mr. Jun Chen, Mr. Yu Wang, Mr. Kun Zhang, and Mr. Lingfei Zhi, for their generous and invaluable help, heartwarming friendships and the happy times we had together during four years of my graduate study.

Finally, I would like to express my eternal gratefulness to my parents and my wife Panpan Hu. Their unconditional love and support from my parents have fueled me with all the confidence and courage to complete my master degree. My wife Panpan Hu is always there supporting me, caring for me, and bringing joy to my life. Truly, this dissertation would not be possible without them.

TABLE OF CONTENTS

LIST OF FIGURES

CHAPTER 1

INTRODUCTION

Most real-world systems comprise multiple interrelated states which are simultaneously affected by multiple control inputs or disturbances. For example, a typical industrial robotic manipulator may contain 6 or even more Degree of Freedoms (DOFs) with multiple actuators. In a chemical plant, there may be hundreds or even thousands of state variables with strong and complicated interactions and various inputs. The simplest airplane has at least three main control surfaces, namely, ailerons, elevator, and rudder to control the roll, pitch, and yaw angles of the aircraft. To improve the flight performance and accomplish certain tasks, secondary control surfaces are employed in advanced modern aircraft, *e.g.,* both Trailing Edge Control Surface (TECS) and Leading Edge Control Surface (LECS) have been applied in the wing section model to suppress aeroelastic flutter and Limit Circle Oscillations (LCOs) that would yield to catastrophic failure. Obviously, all these kinds of Multi-Input Multi-Output (MIMO) systems are complex to model, understand, and control, which makes the MIMO control design much more interesting and challenging than the Single-Input Single Output (SISO) counterpart.

This dissertation presents progress in Lyapunov-based design and engineering application in the research field of MIMO control design for a class of nonlinear MIMO systems. Given different model structures, properties, and performance requirements, robust adaptive control, adaptive output control, model-free control, and continuous robust control design have been proposed and verified in simulation on robot manipulators and aeroelastic models with multiple control surfaces. The future work during the rest of my Ph. D. study will focus on generalizing the continuous robust control design procedure for the systems with arbitrary dimension of input and output and adaptive output-feedback block-backstepping control design for systems with arbitrary relative degree.

CHAPTER 2

BACKGROUND

The control design problem for the minimum phase Linear Time Invariant (LTI) SISO systems with parametric or structure uncertainty has successfully solved as far as twenty years ago [2]. Early results related to the adaptive control design problem for uncertain MIMO linear systems can be found in the work of [2, 3, 4]. Most of these approaches were based on assuming certain properties on High Frequency Gain (HFG) matrix K_p. In [2], K_p was assumed to be known while [5] assumed knowledge of the upper bound of $\|K_p\|$. In [3], the existence of a matrix S_p was assumed such that K_pS_p is positive definite and symmetric. The matrix decomposition approach $K_p = LU$ used in [6] required *apriori* knowledge of the lower bounds of the diagonal entries for the matrix U. By supposing that the signs of the leading principal minors of K_p were known, an adaptive controller was designed for minimum-phase systems with relative degree one in [7], and later extended in [8] to solve MRAC problem for systems with uniform relative degree two by using a matrix decomposition approach which facilitates the ensuing algebraic loop free control design.

For uncertain MIMO nonlinear systems, research has been focused on special classes of such systems. Under the assumption that the control gain matrix is known, adaptive back-

stepping was applied in [9]. For a class of feedback linearizable systems, various controllers were designed in [10, 11, 12]. A general procedure was presented in [13] to design switching adaptive controllers for several classes of systems. In [14], a neural network-based adaptive controller was formulated for a class of MIMO nonlinear systems where the unknown control gain matrix is positive-definite but not symmetric. Three control parametrizations were proposed in [15] to design stable direct MRAC for a class of MIMO linear systems with minimum phase, diagonal interactor, and arbitrary vector relative degree. In [16], adaptive neural controllers were designed for two classes of MIMO systems with block-triangular forms. Later in [17], an adaptive neural controller is proposed for the MIMO nonlinear system with time-varying delay while its dead-zone and gain sign are unknown. When the sign of the high-frequency gain is unknown, an adaptive control is proposed in [18] where the so-called Nussbaum gain was utilized. In [19], the output of a class of MIMO systems was tracked via full-state feedback adaptive control, which achieves global asymptotic convergence for the tracking error. In [20], an adaptive output feedback control was designed to extend the work in [19] but the proposed control law was susceptible to singularities owing to the existence of an algebraic loop in the controller. In [21], a robust adaptive control law was proposed with guaranteed performance through application of an error transformation while neural network approximator was utilized to compensate the unknown nonlinearity in the drift vector and HFG matrix. Later in [22], a robust adaptive switching control law was proposed to solve the Prescribed Performance Adaptive Control (PPAC) problem. An inner loop controller was designed in [23] with guaranteed robust transient performance

through designing a feedback loop that approximates the difference between the system and the nominal model to generate the compensating signal. In [24], a backstepping control law was designed to solve the tracking problem for a class of MIMO system with adaptive mechanism embedded. Applications of control design for MIMO uncertain systems to thermal management, visual servoing, and aeroelasticity can be found in [25, 26, 27, 28].

CHAPTER 3

PROBLEM STATEMENT

For the following general affine in the control nonlinear MIMO system

$$x^{(n)} = h\left(x,\, \dot{x},\, \ddot{x}, ..., x^{(n-1)}\right) + G\left(x,\, \dot{x},\, \ddot{x}, ..., x^{(n-1)}\right) u, \tag{3.1}$$

full state feedback or output feedback control laws are designed given certain properties on the drift vector $h(\cdot)$ and HFG matrix $G(\cdot)$ as well as various performance requirements. Note that in (3.1), $x^{(i)}(t) \in \mathbb{R}^m$, $i = 0, 1, ..., n-1$ are the system states variables while $y(t) = x(t) \in \mathbb{R}^m$ denotes the output. One can further define $\mathbf{x} \triangleq [x^T\ \dot{x}^T\ ...\ (x^{(n-2)})^T]^T \in \mathbb{R}^{mn-m}$ to facilitate the ensuing analysis while $u(t) \in \mathbb{R}^m$ represents the control input signal. We also define a smooth desired trajectory $x_d(t) \in \mathbb{R}^m$ in the sense that

$$x_d^{(i)}(t) \in \mathcal{L}_\infty, \quad i = 0, 1, ..., n+1 \tag{3.2}$$

and $\mathbf{x}_d \triangleq \left[\begin{array}{cccc} x_d^T & \dot{x}_d^T & ... & \left(x_d^{(n-2)}\right)^T \end{array}\right]^T \in \mathbb{R}^{mn-m}$. The drift vector $h\left(\mathbf{x}, x^{(n-1)}\right) \in \mathbb{R}^m$ and HFG matrix $G(\mathbf{x}) \in \mathbb{R}^{m\times m}$ are assumed to be locally Lipschitz in their arguments over the domain of interest in this dissertation. In this dissertation, we suppose that $G(\mathbf{x})$ is a real matrix with nonzero leading principal minors. The control design problems solved in this dissertation are listed as follows:

- Robust adaptive control design without algebraic loop [29]: We address the problem of adaptive control design for a subclass of multi-input multi-output (MIMO) nonlinear systems defined in (4.1). A Lyapunov based singularity free control law, which compensates for parametric uncertainty in both the drift vector and the input gain matrix, is proposed under the mild assumption that the signs of the leading minors of the control input gain matrix are known. Lyapunov analysis shows global uniform ultimate boundedness (GUUB) result for the tracking error under full state feedback. Under the restriction that only the output vector is available for measurement, an output feedback controller is designed based on a standard high gain observer — stability under output feedback is fostered by the uniformity of the full state feedback solution. Simulation results for both full-state and output feedback controllers demonstrate the efficacy of the MIMO control design in the classical 2-DOF robot manipulator model.

- Adaptive output feedback control design and its stability analysis [31]: In this work, an adaptive feedback control is designed for a class of MIMO nonlinear systems containing parametric uncertainty in both the drift vector and the input gain matrix, which is assumed to be full-rank and non-symmetric in general. Based on an SDU decomposition of the gain matrix, a singularity-free adaptive tracking control law is proposed that is shown to be Globally Asymptotically Stable (GAS) under full-state feedback. Output Feedback (OFB) results are facilitated via the use of a high-gain observer (HGO). Under output feedback control, ultimate boundedness of the error signals is obtained – the size of the bound is related to the size of the uncertainty in

the parameters. An explicit upper bound is also provided on the size of the HGO gain constant.

- Model-free MIMO nonlinear control design for an aeroelastic system [30]: In this work, a class of aeroelastic systems with an unmodeled nonlinearity and external disturbance is considered. By using leading- and trailing-edge control surface actuations, a full-state feedforward/feedback controller is designed to suppress the aeroelastic vibrations of a nonlinear wing section subject to external disturbance. The Full State Feedback (FSB) control yields a Uniformly Ultimately Bounded (UUB) result for two-axis vibration suppression. With the restriction that only pitching and plunging displacements are measurable while their rates are not, a HGO is used to modify the full-state feedback control design to an OFB design. Simulation results demonstrate the efficacy of the MIMO control toward suppressing aeroelastic vibration and Limit Cycle Oscillations (LCOs) occurring in pre- and post-flutter velocity regimes when the system is subjected to a variety of external disturbance signals. Comparisons are drawn with a previously designed adaptive MIMO controller.

- Continuous robust control design for 2-DOF MIMO nonlinear system [32]: In this work, a continuous robust feedback control is designed for a class of high-order MIMO nonlinear systems with two degrees of freedom containing unstructured nonlinear uncertainties in the drift vector and parametric uncertainties in the high frequency gain matrix, which is allowed to be non-symmetric in general. Given some mild assumptions on the system model, a singularity-free continuous robust tracking control law

is designed that is shown to be semi-globally asymptotically stable under full-state feedback through a Lyapunov stability analysis. Simulation results demonstrate the efficacy of the proposed control design in a classical 2-DOF robot model. In the special case that G is a unknown constant matrix [33], the proposed control design has been applied to the 2-DOF aeroelastic wing section model to suppress aeroelastic flutter and LCOs.

CHAPTER 4

METHODOLOGY

4.1 Robust Adaptive Control Design

We consider a class of MIMO nonlinear system of the form

$$x^{(n)} = h\left(x, \dot{x}, \cdots, x^{(n-1)}, \theta_1\right) + G\left(x, \dot{x}, \cdots, x^{(n-2)}, \theta_2\right) u \tag{4.1}$$

where $x^{(i)}(t)$, $\mathbf{x}(t)$, $u(t)$ have been defined in (3.1). For the purpose of adaptive control design, we suppose that $h(\cdot)$ and $G(\cdot)$ are affine in the unknown constant parameter vector $\theta_i \in \mathbb{R}^{l_i}\ \forall\ i = 1, 2$. The following matrix decomposition result plays a critical role in the control design

Lemma 1 *Any real matrix $G \in \mathbb{R}^{m\times m}$ with nonzero leading principal minors can be decomposed as [1]*

$$G = SDU \tag{4.2}$$

where $S \in \mathbb{R}^{m\times m}$ is a symmetric positive definite matrix, $D \in \mathbb{R}^{m\times m}$ is a diagonal matrix with diagonal entries $+1$ or -1, $U \in \mathbb{R}^{m\times m}$ is a unity upper triangular matrix. The proof for Lemma 1 can be found in [1].

We make two mild assumptions for the purposes of control design, first that there exists a lower bound for the determinant of S such that $\det(S) \geq \varepsilon > 0$, and second that D is known. Motivated by Lemma 1, (4.1) can be given as

$$M(\mathbf{x}, \theta_2)\, x^{(n)} = \varphi\left(\mathbf{x}, x^{(n-1)}, \theta_1, \theta_2\right) + \det(S)\, DU(\mathbf{x}, \theta_2)\, u \tag{4.3}$$

where $S(\mathbf{x}, \theta_2), U(\mathbf{x}, \theta_2)$, and D have been previously defined. $M(\mathbf{x}, \theta_2) \triangleq adj(S) \in \mathbb{R}^{m \times m}$ is a symmetric and positive definite matrix while $\varphi(\mathbf{x}, x^{(n-1)}, \theta_1, \theta_2) \triangleq adj(S)\, h(\mathbf{x}, x^{(n-1)}, \theta_1) \in \mathbb{R}^m$ is an auxiliary vector. Here, $\det(S)$ can be linearly parameterized as follows

$$\det(S) = y_s(\mathbf{x})\, \theta_s \tag{4.4}$$

where $y_s(\mathbf{x}) \in \mathbb{R}^{1 \times p_2}$ is the regression vector while $\theta_s \in \mathbb{R}^{p_2}$ is the unknown constant parameter vector. We assume that the matrix $M(\cdot)$ is bounded by

$$\underline{m} \|\xi\|^2 \leqslant \xi^T M(\cdot)\, \xi \leqslant \bar{m}(\cdot) \|\xi\|^2 \qquad \forall \xi \in \mathbb{R}^m \tag{4.5}$$

where $\underline{m} \in \mathbb{R}$ denotes a positive constant function and $\bar{m}(\cdot) \in \mathbb{R}$ represents a positive, non-decreasing function.

The control objective is to guarantee the practical convergence of the tracking error as well as to ensure boundedness for all signals during closed-loop operation. The tracking error $e_1 \in \mathbb{R}^m$ is defined as follows

$$e_1 = x_d - x. \tag{4.6}$$

In order to simplify the control design procedure, the following auxiliary error signals are designed as

$$\begin{aligned} e_2 &= \dot{e}_1 + e_1 \\ e_3 &= \dot{e}_2 + e_2 + e_1 \\ e_4 &= \dot{e}_3 + e_3 + e_2 \\ &\vdots \\ e_n &= \dot{e}_{n-1} + e_{n-1} + e_{n-2}. \end{aligned} \tag{4.7}$$

From [34], it is easy to see that

$$e_i(t) = \sum_{j=0}^{i-1} c_{ij} e_1^{(j)}(t) \qquad \forall\ i = 2, 3, ..., n \tag{4.8}$$

where the known constant coefficients c_{ij} are generated via a Fibonacci number series [34]. Furthermore, we define the error signal $r(t) \in \mathbb{R}^m$ and $z(t) \in \mathbb{R}^{mn}$ as follows

$$r = e_n + e_{n-1}, \quad z \triangleq \left[\begin{array}{ccccc} e_1^T & e_2^T & ... & e_{n-1}^T & r^T \end{array}\right]^T. \tag{4.9}$$

By taking the time derivative of r in (4.9), we obtain

$$M\dot{r} = -\frac{1}{2}\dot{M}r + Y\theta - \det(S)\, Du - e_{n-1} \tag{4.10}$$

where the linear parameterization $Y(\cdot)\,\theta \in \mathbb{R}^m$ is defined as follows

$$\begin{aligned} Y(\cdot)\,\theta = \ & M\left(x_d^{(n)} + \sum_{j=0}^{n-2} a_{n,j} e_1^{(j+1)} + \dot{e}_{n-1}\right) - \varphi\left(\mathbf{x}, x^{(n-1)}, \theta_1, \theta_2\right) \\ & + \tfrac{1}{2}\dot{M}r - \det(S)\, D\bar{U}(\mathbf{x}, \theta_2)\, u + e_{n-1} \end{aligned} \tag{4.11}$$

where $Y(\cdot) \in \mathbb{R}^{m \times p_1}$ is a measurable regression matrix while $\theta \in \mathbb{R}^{p_1}$ is the corresponding unknown system parameter vector containing θ_1 and θ_2. Also note that $\bar{U}(\mathbf{x}, \theta_2) = U(\mathbf{x}, \theta_2) - I_m$ is a strictly upper triangular matrix.

Assume that all state variables in (4.1) are available for measurement. We begin by defining the following auxiliary control matrices

$$\begin{aligned} T &= diag\left[||Y_1||^2 \quad \cdots \quad ||Y_m||^2\right] \in \mathbb{R}^{m\times m} \\ R &= diag\left[||y_s||^2||W_1||^2 \quad \cdots \quad ||y_s||^2||W_m||^2\right] \in \mathbb{R}^{m\times m} \end{aligned} \tag{4.12}$$

where y_s has previously been defined in (4.4), $Y_i(\cdot)$ denotes the i^{th} row of the measurable regression matrix $Y(\cdot)$ while $W_i(\cdot)$ denotes the i^{th} row of the following measurable auxiliary control vector

$$W = \left(y_s\hat{\theta}_s\right)^{-1}\left(Y\hat{\theta} + Kr + k_T Tr\right) \in \mathbb{R}^m. \tag{4.13}$$

Based on the open-loop dynamics of (4.10) as well as the subsequent stability analysis, we propose the following state feedback adaptive control law

$$u(t) = D^{-1}\left[\left(y_s\hat{\theta}_s\right)^{-1}\left(Y\hat{\theta} + Kr + k_T Tr\right) + k_R Rr\right] \tag{4.14}$$

where $K \in \mathbb{R}^{m\times m}$ is a positive-definite, diagonal gain matrix while $k_T \in \mathbb{R}$ and $k_R \in \mathbb{R}$ are auxiliary control gains. Motivated by [35], the parameter adaptation law for $\hat{\theta}(t) \in \mathbb{R}^{p_1}$ is given as follows

$$\dot{\hat{\theta}} = \text{Proj1}\left\{\Gamma Y^T r, \hat{\theta}\right\} \tag{4.15}$$

where $\Gamma \in \mathbb{R}^{p_1\times p_1}$ is a constant diagonal, positive definite matrix. The parameter projection operator Proj1$\{\cdot\}$ is designed to bound $\hat{\theta}(t)$ in a known compact set Ω_ε in the sense that

$$\hat{\theta}(t) \in \Omega_\varepsilon \qquad \forall t > 0 \quad \text{if } \hat{\theta}(0) \in \Omega_\varepsilon. \tag{4.16}$$

Similarly, the parameter adaptation law for $\hat{\theta}_s(t) \in \mathbb{R}^{p_2}$ is designed as follows

$$\dot{\hat{\theta}}_s = \text{Proj2}\left\{\Gamma_s \mu\right\}, \quad \mu = -\frac{y_s^T}{y_s\hat{\theta}_s}\left(Y\hat{\theta} + Kr + k_T Tr\right)^T r \tag{4.17}$$

where $\Gamma_s \in \mathbb{R}^{p_2 \times p_2}$ is a constant diagonal, positive definite matrix and Proj2$\{\cdot\}$ is a parameter projection operator as defined in [9] and [36]. This projection operation is used to ensure that $y_s \hat{\theta}_s \geq \varepsilon > 0$ and $\hat{\theta}_s \in \Omega_{\varepsilon s}$ for all time if $\hat{\theta}_s(0) \in \Omega_{\varepsilon s}$. For details, the reader is referred to [19]. The triangular structure of $\bar{U}$ in (4.11) implies that u_i only depends on $u_{i+1}, \ldots, u_m$ while u_m can be determined independently of other control inputs. So, the control law can be implemented by designing u_m first, then using that design in the computation of u_{m-1} and so forth until we finish the control design for u_1. The proposed control design effectively solves the algebraic loop problem of the previous method in [20].

After substituting (4.14) into (4.10), and subsequently multiplying both sides by $M(\mathbf{x},\theta_2)$, one can obtain the following closed-loop system dynamics

$$M\dot{r} = -\frac{1}{2}\dot{M}r - e_{n-1} - Kr + Y\tilde{\theta} - k_T T r - \frac{y_s \tilde{\theta}_s}{y_s \hat{\theta}_s}\left(Y\hat{\theta} + Kr + k_T T r\right) - y_s \theta_s k_R R r \quad (4.18)$$

where $\tilde{\theta}(t)$ and $\tilde{\theta}_s(t)$ are parameter estimation errors defined as follows

$$\tilde{\theta}(t) \triangleq \theta - \hat{\theta}, \quad \tilde{\theta}_s(t) \triangleq \theta_s - \hat{\theta}_s \quad (4.19)$$

In order to analyze the stability of the full state feedback control law in (4.14), we define a non-negative Lyapunov candidate function $V(t,z) \in \mathbb{R}$ as follows

$$V(t,z) = \frac{1}{2}\sum_{i=1}^{n-1} e_i^T e_i + \frac{1}{2} r^T M r \quad (4.20)$$

which can be upper and lower bounded as

$$\alpha_1(\|z\|) \leqslant V \leqslant \alpha_2(\|z\|) \quad (4.21)$$

where $\alpha_1(\|z\|)$ and $\alpha_2(\|z\|)$ are class $\mathcal{K}_\infty$ functions given as

$$\alpha_1(\|z\|) \triangleq \frac{1}{2}\min(1, \underline{m})\|z\|^2, \quad \alpha_2(\|z\|) \triangleq \frac{1}{2}\max(1, \bar{m}(\cdot))\|z\|^2. \tag{4.22}$$

where we have utilized the assumption stated in (4.5). By taking the time derivative of (4.20), and then substituting from (4.7) and (4.18), one can obtain following result for $\dot{V}(t,z)$

$$\begin{aligned}\dot{V} = & -\sum_{i=1}^{n-1} e_i^T e_i - e_{n-1}^T e_{n-1} - r^T K r + r^T\left(Y\tilde{\theta} - k_T T r\right) \\ & -r^T y_s \theta_s k_R R r - r^T \frac{y_s \tilde{\theta}_s}{y_s \hat{\theta}_s}\left(Y\hat{\theta} + Kr + k_T T r\right).\end{aligned} \tag{4.23}$$

By utilizing the expressions given in (4.12) and (4.13), we can rewrite the expression in (4.23) as follows

$$\begin{aligned}\dot{V} \leqslant & -\sum_{i=1}^{n-1} e_i^T e_i - e_{n-1}^T e_{n-1} - r^T K r + \sum_{i=1}^{m}\left(-k_T\|Y_i\|^2\|r_i\|^2 + \left\|\tilde{\theta}\right\|\|Y_i\|\|r_i\|\right) \\ & +\sum_{i=1}^{m}\left(-y_s\theta_s k_R\|y_s\|^2\|W_i\|^2\|r_i\|^2 + \|y_s\|\left\|\tilde{\theta}_s\right\|\|W_i\|\|r_i\|\right).\end{aligned} \tag{4.24}$$

From simple algebraic manipulations, it is clear that the following terms

$$\begin{gathered}\sum_{i=1}^{m}\left(-k_T\|Y_i\|^2\|r_i\|^2 + \left\|\tilde{\theta}\right\|\|Y_i\|\|r_i\|\right), \\ \sum_{i=1}^{m}\left(-y_s\theta_s k_R\|y_s\|^2\|W_i\|^2\|r_i\|^2 + \|y_s\|\left\|\tilde{\theta}_s\right\|\|W_i\|\|r_i\|\right)\end{gathered} \tag{4.25}$$

reach their maximum value at

$$\sqrt{k_T}\|Y_i\|\|r_i\| = \frac{\left\|\tilde{\theta}\right\|}{2\sqrt{k_T}} \text{ and } \sqrt{y_s\theta_s k_R}\|y_s\|\|W_i\|\|r_i\| = \frac{\left\|\tilde{\theta}_s\right\|}{2\sqrt{y_s\theta_s k_R}} \tag{4.26}$$

$\forall\ i = 1...m$. Thus, $\dot{V}(t,z)$ can be further upperbounded as

$$\dot{V} \leq -\left(\sum_{i=1}^{m-1} e_i^T e_i + e_{n-1}^T e_{n-1} + r^T K r\right) + \sum_{i=1}^{m}\left(\frac{\left\|\tilde{\theta}\right\|^2}{4k_T} + \frac{\left\|\tilde{\theta}_s\right\|^2}{4\det(S)k_R}\right) \tag{4.27}$$

where we have utilized the fact $\det(S) = y_s\theta_s$. Based on the definition of $z(t)$ given in (4.9), $\dot{V}(t,z)$ of (4.27) can be further upperbounded as follows

$$\dot{V} \leqslant -\lambda_3 \|z\|^2 + \delta \tag{4.28}$$

where $\lambda_3 \triangleq \min\{1, \lambda_{\min}(K)\}$, $\lambda_{\min}(K)$ denotes the minimum eigenvalue of K, while δ is given by

$$\delta = \sum_{i=1}^{m} \left(\frac{\varepsilon\delta_1 + \delta_2}{4\varepsilon k} \right), \quad k = \min(k_T,\ k_R) \tag{4.29}$$

In the above expression, ε is the aforementioned lower bound for $\det(S)$ while $\delta_1, \delta_2 \in \mathbb{R}$ are positive constants defined as follows

$$\delta_1 = \sup_{\hat{\theta}\in\Omega_\varepsilon} \left\|\tilde{\theta}\right\|^2, \quad \delta_2 = \sup_{\hat{\theta}_s\in\Omega_{\varepsilon s}} \left\|\tilde{\theta}_s\right\|^2 \tag{4.30}$$

where the supremum exist due to the boundedness of the parameter estimates resulting from the parameter projection operators defined in (4.15) and (4.17). From (4.28), it is also easy to show that

$$\dot{V} \leqslant -\gamma(\|z\|), \quad \forall \|z\| > \varsigma > 0 \tag{4.31}$$

where $\varsigma = \sqrt{\lambda_3^{-1}\delta}$ while $\gamma(\|z\|)$ is a function that assumes positive values. From the results in (4.22) and (4.31), all conditions for Theorem 4.18 in [37] are satisfied. So one can easily draw the conclusion that error signal $\|z\|$ is Globally Uniformly Ultimately Bounded (GUUB) in the sense that

$$\begin{gathered} \|z\| < \beta(\|z_0\|,\ t - t_0),\ \forall t_0 < t \leq t_0 + T \\ \|z\| \leq \alpha_1^{-1}(\alpha_2(\varsigma)),\ \forall t \geq t_0 + T \end{gathered} \tag{4.32}$$

where $\beta(\cdot,\cdot)$ is a class $\mathcal{KL}$ function while T depends on $\|z_0\|$ and ς. From (4.29), it is clear that the upper bound for $\|z\|$ can be made arbitrarily small by choosing k large enough. Also note that similar results can be obtained by using Theorem 2.15 in [38].

Remark 1 *We remark here that it is possible to augment the Lyapunov function of (4.20) with quadratic terms related to the parameter estimation errors $\tilde{\theta}(t)$ and $\tilde{\theta}_s(t)$ in order to foster a global asymptotic stability (GAS) result — instead, a UUB result is obtained here via the damping of the estimation error through nonlinear injection of the terms $D^{-1}\left(y_s\hat{\theta}_s\right)^{-1}k_T Tr$ and $D^{-1}k_R Rr$ in the control design given in (4.14). The GAS result is not pursued because the subsequent output feedback control design is fostered by the uniformity of the result obtained here. Thus, asymptotic convergence under state feedback is sacrificed here in order to obtain uniform practical convergence under state and subsequently output feedback.*

When the only available measurement is the system output vector while all other system states are not measurable, the error signal $z(t)$ can be obtained from estimating

$$\hat{z}(t) = \begin{bmatrix} \hat{e}_1^T & \hat{e}_2^T & \cdots & \hat{e}_{n-1}^T & \hat{r}^T \end{bmatrix}^T \in \mathbb{R}^{mn} \tag{4.33}$$

through use of the following high gain observer (HGO) [39]

$$\begin{aligned}
\dot{\hat{e}}_1 &= \hat{e}_2 - \hat{e}_1 + \frac{a_1}{\epsilon}(e_1 - \hat{e}_1) \\
\dot{\hat{e}}_2 &= \hat{e}_3 - \hat{e}_2 - \hat{e}_1 + \frac{a_2}{\epsilon^2}(e_1 - \hat{e}_1) \\
&\vdots \\
\dot{\hat{e}}_{n-1} &= \hat{r} - 2\hat{e}_{n-1} - \hat{e}_{n-2} + \frac{a_{n-1}}{\epsilon^{n-1}}(e_1 - \hat{e}_1) \\
\dot{\hat{r}} &= \frac{a_n}{\epsilon^n}(e_1 - \hat{e}_1)
\end{aligned} \tag{4.34}$$

For the details of the determination of $a_i \in \mathbb{R}^{m\times m}\ \forall\ i = 1, 2, \cdots, n$ and ϵ, the reader is referred to [39].

Although the High Gain Observer (HGO) is a powerful tool in solving state estimation problems and is widely used in numerous fields, it also suffers from a serious drawback, namely the peaking phenomenon, due to the use of high gain. In order to suppress the amplitude peaking, we modify the full-state control design of (4.14) to an output feedback saturated control

$$u(t) = D^{-1}\left[\left(\hat{y}_s\hat{\theta}_s\right)^{-1}\left[\hat{Y}\hat{\theta} + K\text{sat}\left\{\hat{r}\right\} + k_T\hat{T}\text{sat}\left\{\hat{r}\right\}\right] + k_R\hat{R}\text{sat}\left\{\hat{r}\right\}\right] \tag{4.35}$$

where $\text{sat}\{\cdot\}$ denotes a standard saturation function, $\hat{y}_s(\cdot), \hat{Y}(\cdot), \hat{T}(\cdot)$, and $\hat{R}(\cdot)$ are the same measurable regressor and auxiliary control signals defined in (4.4), (4.11), and (4.12) with respect to $\text{sat}\{\hat{z}(t)\}$, while K, k_T and k_R are control gains that have been previously defined. Here, the saturation is applied in the variable $\hat{z}(t)$ outside a compact set. In (4.35), $\hat{\theta}(t)$ and $\hat{\theta}_s(t)$ are generated by the projection algorithm in (4.15) and (4.17) with respect to $\hat{Y}(t)$ and $\text{sat}\{\hat{r}(t)\}$

$$\begin{aligned}
&\dot{\hat{\theta}} = \text{Proj1}\left\{\Gamma\hat{Y}^T\text{sat}\{\hat{r}\}, \hat{\theta}\right\}, \quad \dot{\hat{\theta}}_s = \text{Proj2}\left\{\Gamma_s\hat{\mu}\right\} \\
&\hat{\mu} = -\frac{\hat{y}_s^T}{\hat{y}_s\hat{\theta}_s}\left(\hat{Y}\hat{\theta} + K\text{sat}\{\hat{r}\} + k_T\hat{T}\text{sat}\left\{\hat{r}\right\}\right)^T\text{sat}\{\hat{r}\}
\end{aligned} \tag{4.36}$$

For details of the stability analysis of the output feedback control design, the reader is referred to [20].

In the simulation, the following two DOF robot manipulator model has been considered [40]

$$\begin{bmatrix} \tau_1 \\ \tau_2 \end{bmatrix} = \begin{bmatrix} H_{11} & H_{12} \\ H_{21} & H_{22} \end{bmatrix} \begin{bmatrix} \ddot{q}_1 \\ \ddot{q}_2 \end{bmatrix} + \begin{bmatrix} -h\dot{q}_2 & -h(\dot{q}_1 + \dot{q}_2) \\ h\dot{q}_1 & 0 \end{bmatrix} \begin{bmatrix} \dot{q}_1 \\ \dot{q}_2 \end{bmatrix} \tag{4.37}$$

where $q_i(t)$ denotes the i^{th} DOF position. $H_{11} = a_1 + 2a_3 \cos q_2 + 2a_4 \sin q_2$, $H_{12} = H_{21} = a_2 + a_3 \cos q_2 + a_4 \sin q_2$, $H_{22} = a_2$, $h = a_3 \sin q_2 - a_4 \sin q_2$. The control input is defined as

$$\begin{bmatrix} \tau_1 \\ \tau_2 \end{bmatrix} = a(q_1, q_2) \begin{bmatrix} 1 & 1 \\ 0 & 1 \end{bmatrix} \begin{bmatrix} u_1 \\ u_2 \end{bmatrix}, \tag{4.38}$$

$$a(q_1, q_2) = H_{11}H_{22} - H_{12}H_{21}$$

where $a_1 = 4.42$, $a_2 = 0.97$, $a_3 = 1.04$, and $a_4 = 0.60$. In (4.38), $u_1(t)$, $u_2(t)$ are the control inputs. $a(q_1,q_2)$ is a scalar function, which can be considered as a sort of environment related factor (as in [41]), or items shown in the input-output module, e.g., see [36] and [42]. The control objective is to make $q(t) = \begin{bmatrix} q_1(t) & q_2(t) \end{bmatrix}^T$ track the following reference trajectory $q_d(t) = (1 - e^{-0.3t^3}) \begin{bmatrix} 30\sin(t) & 45\sin(t) \end{bmatrix}$ deg. The initial conditions of the robot manipulator are set to $q_1(0) = q_2(0) = 0.05\,\text{rad}$ and $\dot{q}_1(0) = \dot{q}_2(0) = 0\,\text{rad}\,.\,\text{s}^{-1}$. The control gains in (4.14) have been chosen to be $K = diag\{7.5, 4.5\}$, $k_T = 0.1$, and $k_R = 0.1$ through trial-and-error method. In (4.36), the gains for the adaptive parameter estimation law are chosen as $\Gamma = 0.01 I_9$ and $\Gamma_s = I_3$. The parameter estimates are initialized to the following values: $\hat{\theta}(0) = [4.42, 0.97, 1.04, 0.60, 4.28, 0.62, 0.94, 1.08, 0.36]^T$, $\hat{\theta}_s(0) = \begin{bmatrix} 2.98 & 1.08 & 1.25 \end{bmatrix}^T$. In the FSFB scenario, Figure 4.1 shows the output tracking errors defined as $e = q_d(t) - q(t)$. Fig. 4.2 shows the control input defined in (4.14). Fig. 4.3 shows a sampling of the results from the parameter estimation (space constraints prevent us from showing all estimates). In

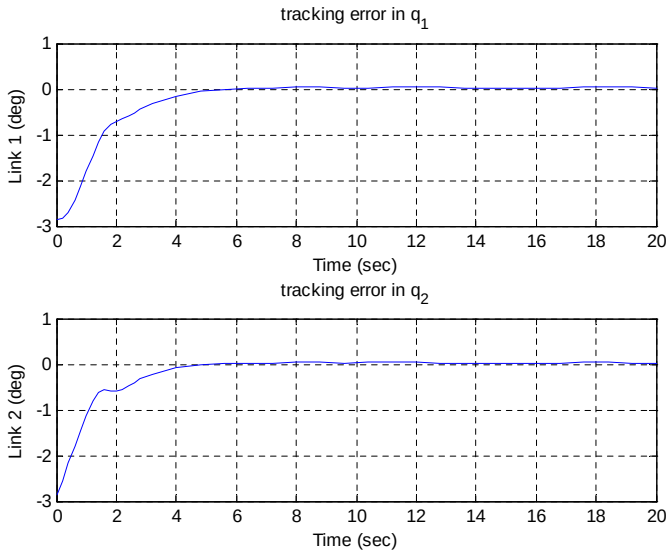

Figure 4.1: Tracking Error under FSFB Control Input.

the OFB scenario, supposing that there is no sensor noise and sampling frequency is infinite, we implement the HGO in (4.34) with parameters settings: $n = 2$, $a_1 = 0.91I_2$, $a_2 = 0.15I_2$, and $\varepsilon = 0.0029$ obtained by trial and error. The maximum and minimum values for the saturation for $\hat{z}(t)$ are set at ± 100. The simulation results show that the performance of the FSFB control can be recovered by using the OFB control. Fig. 4.4 shows the tracking errors. Fig. 4.5 shows the control input defined in (4.35). The parameter estimation results under output feedback can be seen in Fig. 4.6.

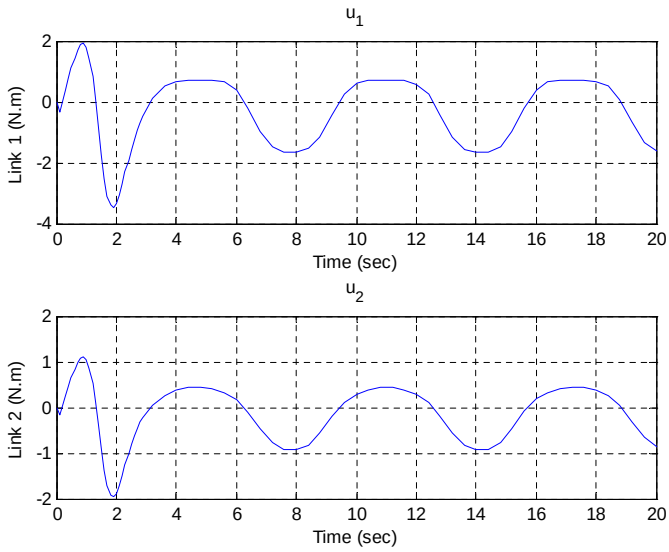

Figure 4.2: FSFB Control Input.

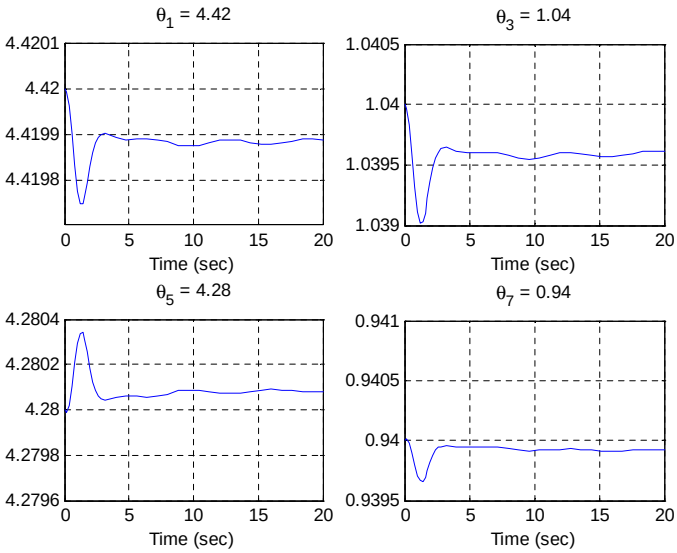

Figure 4.3: Samples of Parameter Estimates under FSFB Control Input.

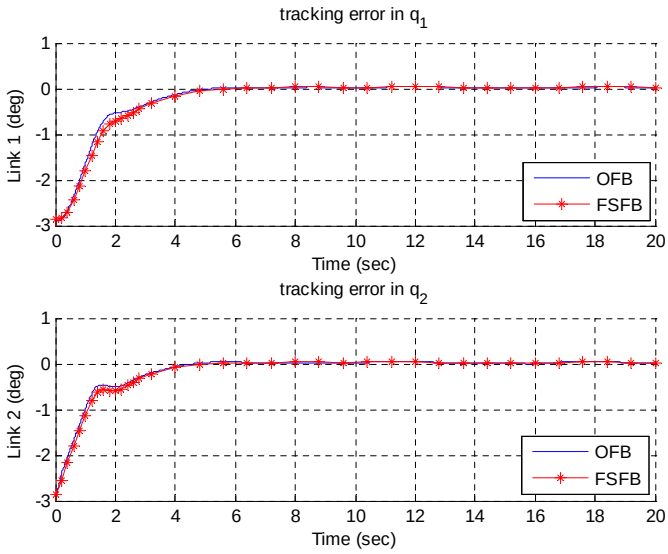

Figure 4.4: Tracking Error Comparison between FSFB and OFB Control Input.

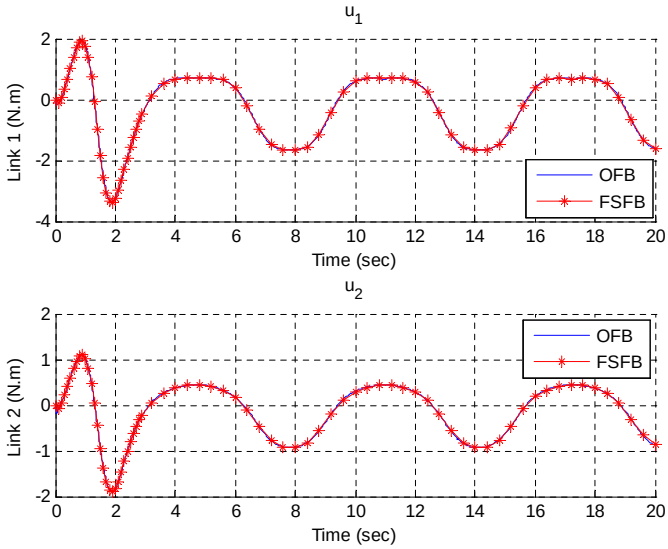

Figure 4.5: Control Input Comparison between FSFB and OFB.

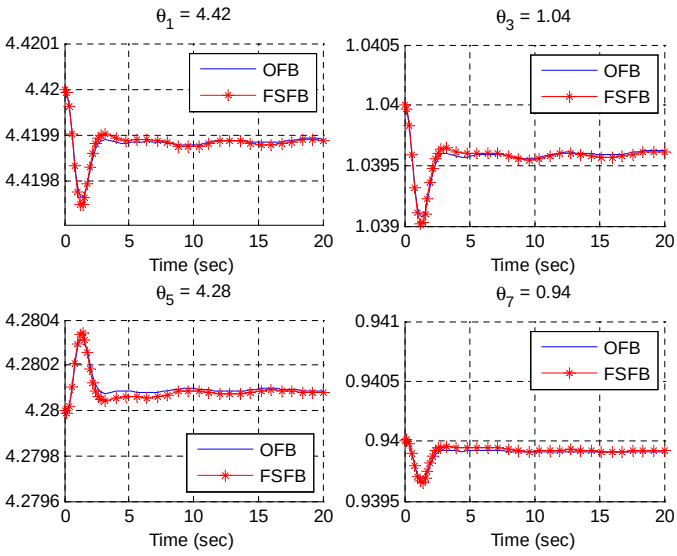

Figure 4.6: Samples of Parameter Estimate Comparison between FSFB and OFB.

4.2 Adaptive Output Feedback Control Design

In the adaptive output feedback control design problem, the MIMO nonlinear system defined in (4.1) is considered. Following the same procedure from (4.3) to (4.11) and taking advantage of (4.8), the system open-loop dynamics can be compactly written as follows

$$\dot{z}(t) = Az + B\dot{r} \tag{4.39}$$

where $z \triangleq [\ e_1^T \quad e_2^T \quad ... \quad e_{n-1}^T \quad r^T\ ]^T \in \mathbb{R}^{mn}$, $A \in \mathbb{R}^{mn\times mn}$, and $B \in \mathbb{R}^{mn\times m}$ are defined as follows

$$A \triangleq \begin{bmatrix} -I_m & I_m & 0_m & \cdots & 0_m & 0_m \\ -I_m & -I_m & I_m & \cdots & 0_m & 0_m \\ 0_m & -I_m & -I_m & \cdots & 0_m & 0_m \\ \vdots & \vdots & \vdots & \ddots & \vdots & \vdots \\ 0_m & 0_m & 0_m & \cdots & -2I_m & I_m \\ 0_m & 0_m & 0_m & \cdots & 0_m & 0_m \end{bmatrix} \tag{4.40}$$

$$B \triangleq \begin{bmatrix} 0_m & 0_m & 0_m & \cdots & 0_m & I_m \end{bmatrix}^T$$

We firstly consider control design via full state feedback, *i.e.*, we assume that $x^{(i)}(t)$, $i = 0, ..., n-1$ in (4.1) are measurable. Based on the open-loop dynamics of (4.10), (4.39), and the subsequent stability analysis, the following state feedback adaptive control law is proposed

$$u(t) = D^{-1}\left[\left(y_s\hat{\theta}_s\right)^{-1}\left(Y\hat{\theta} + Kr\right)\right] \tag{4.41}$$

where $K \in \mathbb{R}^{m\times m}$ is a positive-definite, constant diagonal control gain matrix. The parameter adaptation laws for $\hat{\theta}(t)$ and $\hat{\theta}_s(t)$ are designed as follows

$$\dot{\hat{\theta}} = \text{Proj1}\left\{\Gamma Y^T r, \hat{\theta}\right\}, \quad \dot{\hat{\theta}}_s = \text{Proj2}\left\{\Gamma_s \mu\right\} \tag{4.42}$$

where $\mu = -y_s^T\left(Y\hat{\theta} + Kr\right)^T\left(y_s\hat{\theta}_s\right)^{-1} r$ while $\Gamma \in \mathbb{R}^{q\times q}$ and $\Gamma_s^{p\times p} \in \mathbb{R}$ are constant diagonal, positive definite matrices. Here, Proj1$\{\cdot\}$ is a parameter projection operator defined in [35] which is employed in order to bound $\hat{\theta}(t)$ to a known compact set Ω_θ in the sense that

$\hat{\theta}(t) \in \Omega_\theta,\ \forall t > 0$ if $\hat{\theta}(0) \in \Omega_\theta$ while Proj2$\{\cdot\}$ is a parameter projection operator [9, 36] used to ensure that (a) $y_s\hat{\theta}_s > \delta_s > 0$, and (b) the estimate $\hat{\theta}_s$ stays inside a hypercube convex set denoted by $\Omega_{\theta_s}\ \forall t > 0$ if $\hat{\theta}_s(0) \in \Omega_{\theta_s}$. For details, the reader is referred to [19]. After substituting (4.41) in (4.10), the closed-loop system dynamics for r can be obtained as

$$M\dot{r} = -\frac{1}{2}\dot{M}r + Y\tilde{\theta} - e_{n-1} - Kr - \frac{y_s\tilde{\theta}_s\left(Y\hat{\theta} + Kr\right)}{y_s\hat{\theta}_s} \tag{4.43}$$

where $\tilde{\theta}(t) \triangleq \theta - \hat{\theta}$ and $\tilde{\theta}_s(t) \triangleq \theta_s - \hat{\theta}_s$ are parameter estimation errors. Based upon the boundedness of the parameters and the estimates (owing to the projection laws of (4.42)), the parameter estimation errors $\tilde{\theta}(t)$ and $\tilde{\theta}_s(t)$ belong, respectively, to compact sets $\tilde{\Omega}_\theta$ and $\tilde{\Omega}_{\theta_s}$. In order to analyze the stability of the proposed control law, a non-negative function $V_0(t, \bar{z}) \in \mathbb{R}$ is defined as follows

$$V_0(t, \bar{z}) = \frac{1}{2}\sum\nolimits_{i=1}^{n-1} e_i^T e_i + \frac{1}{2}r^T M r + \frac{1}{2}\tilde{\theta}^T\Gamma^{-1}\tilde{\theta} + \frac{1}{2}\tilde{\theta}_s^T\Gamma_s^{-1}\tilde{\theta}_s \tag{4.44}$$

where $\bar{z} \triangleq \begin{bmatrix} z^T & \tilde{\theta}^T & \tilde{\theta}_s^T \end{bmatrix}^T$. Note that (4.44) can be upper and lower bounded as

$$\lambda_1 \|\bar{z}\|^2 \leqslant V_0 \leqslant \lambda_2(\|\bar{z}\|)\|\bar{z}\|^2 \tag{4.45}$$

where $\lambda_1 \triangleq \frac{1}{2}\min(1, \underline{m}, \Gamma^{-1}, \Gamma_s^{-1})$ and $\lambda_2(\|\bar{z}\|) \triangleq \frac{1}{2}\max(1, \bar{m}(\cdot), \Gamma^{-1}, \Gamma_s^{-1})$. After differentiating (4.44) along (4.42) and (4.43), one can obtain the following upperbound for $\dot{V}_0(t, \bar{z})$

$$\dot{V}_0(t, \bar{z}) \leq -\sum\nolimits_{i=1}^{n-1} e_i^T e_i - r^T K r \leq -\lambda_3 \|z\|^2 \tag{4.46}$$

where $\lambda_3 \triangleq \min\{1, \lambda_{\min}(K)\}$ with $\lambda_{\min}(K)$ denotes the minimum eigenvalue of K and we have taken advantage of the fact that the projection operator ensures that $\tilde{\theta}^T\left(Y^T r - \Gamma^{-1}\dot{\hat{\theta}}\right) \leq$

0 and that $\tilde{\theta}_s^T \left(\mu - \Gamma_s^{-1}\dot{\hat{\theta}}_s\right) \leq 0$. From (4.44) and (4.46), it can be seen that $r(t), e_i(t) \in \mathcal{L}_\infty \cap \mathcal{L}_2, \ \forall \ i = 1, ..., n-1$ while $\tilde{\theta}_s(t), \tilde{\theta}(t) \in \mathcal{L}_\infty$. From (4.8), $e_n(t) \in \mathcal{L}_\infty \cap \mathcal{L}_2$. Given $x_d^{(i)}(t) \in \mathcal{L}_\infty, \ \forall \ i = 0, 1, ..., n$, it can now be seen that $x^{(i)}(t) \in \mathcal{L}_\infty, \ \forall \ i = 0...n-1$. From the aforementioned boundedness claims, one can start from $i = m$ and prove that $u_i(t) \in \mathcal{L}_\infty, \ \forall \ i = 1, ..., m$ by taking advantage of the fact that each $u_k(t)$ only depends upon $u_j(t), \ \forall \ j = k+1, ..., m$. Using (4.42)-(4.43), it can be seen that $\dot{\hat{\theta}}(t), \dot{\hat{\theta}}_s(t)$, and $\dot{r}(t) \in \mathcal{L}_\infty$. From the previous boundedness assertions and the definitions in (4.8), it can be seen that $\dot{e}_i(t) \in \mathcal{L}_\infty, \ \forall \ i = 1, ..., n$. Since $\forall \ i = 1, ..., n$, $r(t), e_i(t) \in \mathcal{L}_\infty \cap \mathcal{L}_2$ and $\dot{r}(t), \dot{e}_i(t) \in \mathcal{L}_\infty$, one can utilize Barbalat's Lemma [40] to prove global asymptotic stability in the sense that $\lim_{t\to\infty} r(t), e_i(t) = 0, \ \forall \ i = 1, ..., n$.

To facilitate the stability analysis under OFB control, we are motivated to demonstrate the uniform boundedness of the closed-loop solution under FSFB control. It is easy to see that the upperbound on $\dot{V}_0$ obtained in (4.46) can be manipulated as follows

$$\dot{V}_0(t, \bar{z}) \leqslant -\sum_{i=1}^{n-1} e_i^T e_i - r^T K r - \tilde{\theta}^T \tilde{\theta} - \tilde{\theta}_s^T \tilde{\theta}_s + \delta_0 \tag{4.47}$$

where $\delta_0 \triangleq \max_{\tilde{\theta} \in \tilde{\Omega}_\theta} \tilde{\theta}^T \tilde{\theta} + \max_{\tilde{\theta}_s \in \tilde{\Omega}_{\theta_s}} \tilde{\theta}_s^T \tilde{\theta}_s$. Then, (4.47) can be further upperbounded to obtain the following inequality

$$\dot{V}_0(t, \bar{z}) \leqslant -\lambda_3 \|\bar{z}\|^2 + \delta_0 \tag{4.48}$$

where λ_3 has been defined previously in (4.46). From (4.48), it is easy to see that the upperbound on $\dot{V}_0(t, \bar{z})$ can be compactly represented as follows

$$\dot{V}_0(t, \bar{z}) \leqslant -\gamma(\|\bar{z}\|), \quad \left\{\bar{z} \in \mathbb{R}^{mn} \times \tilde{\Omega}_\theta \ \times \tilde{\Omega}_{\theta_s} | \lambda_3^{-1} \delta_0 < ||\bar{z}(t)||^2 < \infty\right\} \tag{4.49}$$

where $\gamma(\cdot) : \mathbb{R}^+ \longrightarrow \mathbb{R}^+$ denotes a function that assumes positive values. Given the bound in (4.45) and (4.49), uniform boundedness of the closed loop solution can be obtained in the sense of Theorem 2.15 in [38].

Assuming $x(t)$ as the only measurable state, the measurable error signal $e_1(t)$ can be obtained through the high-gain observer defined in (4.34) in order to obtain an estimate $\hat{z}(t) \triangleq \begin{bmatrix} \hat{e}_1^T & \cdots & \hat{e}_{n-1}^T & \hat{r}^T \end{bmatrix}^T \in \mathbb{R}^{mn}$. To make for facile analysis in the singularly perturbed form, we further define scaled observer errors $\eta(t) \triangleq \begin{bmatrix} \eta_1^T & \eta_2^T & \cdots & \eta_n^T \end{bmatrix}^T \in \mathbb{R}^{mn}$ as follows

$$\begin{aligned} \eta_i(t) &= \frac{1}{\epsilon^{n-i}}(e_i - \hat{e}_i) \quad \forall i = 1, 2, \cdots, n-1; \\ \eta_n(t) &= r - \hat{r} \end{aligned} \tag{4.50}$$

where $\hat{z} = z - D_\eta \eta$ while $D_\eta \triangleq diag\left\{ \epsilon^{n-1} I_m \quad \epsilon^{n-2} I_m \quad \cdots \quad \epsilon I_m \quad I_m \right\} \in \mathbb{R}^{mn \times mn}$ is a diagonal gain matrix. After taking advantage of the design of (4.34) and differentiating (4.50), one can compactly write the dynamics for the observer error system as follows

$$\epsilon \dot{\eta}(t) = A_0 \eta(t) + \epsilon g(\cdot) \tag{4.51}$$

where $A_0 \in \mathbb{R}^{mn\times mn}$ and $g(\cdot) \in \mathbb{R}^{mn}$ are given as

$$\begin{aligned} A_0 &\triangleq \begin{bmatrix} -\alpha_1 I_m & I_m & 0_m & \cdots & 0_m \\ -\alpha_2 I_m & 0_m & I_m & \cdots & 0_m \\ \vdots & \vdots & \vdots & \ddots & \vdots \\ -\alpha_{n-1} I_m & 0_m & 0_m & \cdots & I_m \\ -\alpha_n I_m & 0_m & 0_m & \cdots & 0_m \end{bmatrix} \\ g &\triangleq -\begin{bmatrix} \eta_1^T & \epsilon\eta_1^T + \eta_2^T & \cdots & \epsilon\eta_{n-2}^T + 2\eta_{n-1}^T & -\dot{r}^T \end{bmatrix}^T \end{aligned} \tag{4.52}$$

where the constants $\alpha_i \; \forall \; i = 1, 2, \cdots, n$ are chosen such that A_0 is Hurwitz. The boundary-layer system $\dfrac{d\eta(\tau)}{d\tau} = A_0\eta(\tau)$ (obtained by applying a change of variable $\tau = t/\epsilon$ and then setting $\epsilon = 0$) induces a Lyapunov function $W(\eta) = \eta^T P_0 \eta$ that satisfies the following properties

$$\begin{cases} \lambda_{\min}(P_0)\left\|\eta\right\|^2 \leqslant W(\eta) \leqslant \lambda_{\max}(P_0)\left\|\eta\right\|^2, \\ \dot{W} = \frac{\partial W}{\partial \eta}\dot{\eta} \leqslant -\left\|\eta\right\|^2, \left\|\frac{\partial W}{\partial \eta}\right\| \leqslant 2\left\|P_0\right\|\left\|\eta\right\|. \end{cases} \tag{4.53}$$

where $\left\|P_0\right\| \triangleq \lambda_{\max}(P_0)$. In the above equation, $\lambda_{\max}(P_0)$ denotes the maximum eigenvalue of $P_0 \in \mathbb{R}^{mn\times mn}$ which is a p.d. matrix that satisfies $P_0 A_0 + A_0^T P_0 = -I_{mn}$. From (4.53), it is clear that $\eta(t) = 0$ is a globally exponentially stable equilibrium of the boundary-layer system.

From (4.51), the existence of $\dfrac{1}{\epsilon}e^{-\omega t/\epsilon}$ in the solution of $\eta(t)$ for some $\omega > 0$ may cause so called peaking phenomenon that can drive an OFB controller out of its region of attraction, thereby finally causing instability. To reduce this destabilizing effects, we adapt the approach

mentioned in [39] by modifying (4.41) to an output feedback saturated control law as

$$u(t) = D^{-1}\left[\left(\hat{y}_s\hat{\theta}_s\right)^{-1}\left[\hat{Y}\hat{\theta} + K\text{sat}\left\{\hat{r}\right\}\right]\right] \tag{4.54}$$

where $\text{sat}\{\cdot\}$ denotes a saturation function. $\hat{y}_s(\cdot)$ and $\hat{Y}(\cdot)$ are the same partial measurable regression vector and matrix defined in (4.11) with respect to $\text{sat}\{\hat{z}(t)\}$ instead of $z(t)$. Here, the saturation is applied in the variable $\hat{z}(t)$ outside a compact set $\mathcal{D}_c \triangleq \{\bar{z} \in \mathbb{R}^{mn} \times \tilde{\Omega}_\theta \times\tilde{\Omega}_{\theta_s} |\ V_0(t,\bar{z}) \leqslant c\}$ where $\bar{z}$, $\tilde{\Omega}_\theta$, and $\tilde{\Omega}_{\theta_s}$ have been previously defined. Motivated by the ensuing stability analysis, c is chosen to be a bounded positive constant such that $c > 2\delta_0/\lambda_4$ where

$$\delta_0 \triangleq \max_{\tilde{\theta}\in\tilde{\Omega}_\theta} \tilde{\theta}^T\tilde{\theta} + \max_{\tilde{\theta}_s\in\tilde{\Omega}_{\theta_s}} \tilde{\theta}_s^T\tilde{\theta}_s, \quad \lambda_4 \triangleq \frac{\lambda_3 \min\left(1, \underline{m}, \Gamma^{-1}, \Gamma_s^{-1}\right)}{\max\left(1, \bar{m}(\cdot), \Gamma^{-1}, \Gamma_s^{-1}\right)} \tag{4.55}$$

where $\underline{m}$, $\bar{m}$, and λ_3 have been defined previously in (4.5) and (4.46). In (4.54), $\hat{\theta}(t)$ and $\hat{\theta}_s(t)$ are generated by the same projection algorithms as defined in (4.42) but with respect to $\hat{Y}(t)$ and $\text{sat}\{\hat{r}(t)\}$

$$\dot{\hat{\theta}} = \text{Proj1}\left\{\Gamma\hat{Y}^T\text{sat}\{\hat{r}\}, \hat{\theta}\right\}, \quad \dot{\hat{\theta}}_s = \text{Proj2}\left\{\Gamma_s\hat{\mu}\right\} \tag{4.56}$$

where $\hat{\mu} = -\hat{y}_s^T\left(\hat{Y}\hat{\theta} + K\text{sat}\{\hat{r}\}\right)^T\left(\hat{y}_s\hat{\theta}_s\right)^{-1}\text{sat}\{\hat{r}\}$. Furthermore, $\hat{\theta}(t) \in \Omega_\theta$, $\hat{\theta}_s(t) \in \Omega_{\theta_s}$ and $\hat{y}_s\hat{\theta}_s > \delta_s > 0\ \forall t > 0$ if $\hat{\theta}(0) \in \Omega_\theta$ and $\hat{\theta}_s(0) \in \Omega_{\theta_s}$. After substituting (4.54) into (4.43), one can obtain

$$\begin{aligned} \dot{r} &\triangleq \phi(z, D_\eta\eta, t) \\ &= M^{-1}\left[-\frac{1}{2}\dot{M}r + Y\theta - \frac{y_s\theta_s}{\hat{y}_s\hat{\theta}_s}\left(\hat{Y}\hat{\theta} + K\text{sat}\left\{\hat{r}\right\}\right) - e_{n-1}\right]. \end{aligned} \tag{4.57}$$

After combining (4.39), (4.51), and (4.57), the closed-loop error dynamics for (4.1) are given by the adaptation dynamics in (4.56) as well as the following set of equations

$$\begin{cases} \dot{z}(t) & = f_r(\bar{z}(t), D_\eta \eta(t), t) \triangleq Az + B\phi\left(\bar{z}, D_\eta \eta, t\right) \\ \epsilon\dot{\eta}(t) & = A_0\eta(t) + \epsilon g(\bar{z}(t), D_\eta \eta(t)) \end{cases} \tag{4.58}$$

where the matrices $A, B, A_0, g\left(\cdot\right)$, and $\phi\left(\cdot\right)$ have been defined previously. By taking advantage of the boundedness of the state variables inside the compact set $\mathcal{D}_c$ as well as the saturation of the estimates, it is clear to see from (4.56), (4.57), and (4.58) that $||f_r(z(t), \eta(t))|| \leqslant k_1$, $\left\|\dot{\hat{\theta}}\right\| \leqslant k_2$, and $\left\|\dot{\hat{\theta}}_s\right\| \leqslant k_3$. Here, k_1, k_2, k_3 are positive constants independent of ϵ.

Since the proof of stability of (4.56) and (4.58) is non-trivial owing to the augmented set of dynamics as well as saturation introduced in the OFB design, proof is split into multiple steps (as similarly done in [39]) to reduce the complexity at each step. In the first step, we prove the existence of a positively invariant set $\Sigma \triangleq \mathcal{D}_c \times \mathcal{D}_\epsilon$ for the solutions of (4.56) and (4.58) — here, $\mathcal{D}_c$ has been previously defined, $\mathcal{D}_\epsilon \triangleq \{\eta(t) \in \mathbb{R}^{mn} \mid W(\eta\left(t\right)) \leqslant \varrho\epsilon^2\}$ is a compact set for $\eta(t)$ where $W(t)$ was defined in (4.53), ϱ is a positive constant that is yet to be selected, while ϵ is the HGO constant. In the second step (Theorem 2), we regain the boundedness of solutions of (4.58) provided the trajectory $\left(\bar{z}\left(t\right), \hat{z}\left(t\right)\right)$ starts inside $\mathcal{Z} \times \mathcal{H}$ — here, $\mathcal{Z}$ is defined to be any compact set such that $\mathcal{Z} \subset \mathcal{D}_c$ while $\mathcal{H}$ is defined to be any compact set in the interior of $\mathbb{R}^{mn}$. Then, it can be shown that the HGO constant ϵ can be chosen small enough to ensure that any trajectory of $\left(\bar{z}\left(t\right), \hat{z}\left(t\right)\right)$ starting in the aforementioned compact subset results in $\eta\left(t\right)$ entering the invariant set Σ before $\bar{z}\left(t\right)$ can

escape. In this step, we also provide an explicit upperbound on ϵ. In the final step, we prove the ultimate boundedness of solutions of (4.58).

Theorem 1 ***(Invariant Set Theorem)*** *Given $\Sigma \triangleq \mathcal{D}_c \times \mathcal{D}_\epsilon$, there exists an $\bar{\epsilon}_1 > 0$ such that $\forall\ \epsilon \in (0, \bar{\epsilon}_1]$, Σ is a positively invariant set for the trajectory $(\bar{z}(t), \eta(t))$.*

Proof. Given a composite Lyapunov candidate function $V_c(t, \bar{z})$ as

$$V_c(t, \bar{z}, \eta) = V_0(t, \bar{z}) + W(\eta) \tag{4.59}$$

where V_0 and W have been previously defined in (4.44) and (4.53). Inside the set $\Sigma = \mathcal{D}_c \times \mathcal{D}_\epsilon$, saturation does not apply. After differentiating $V_0(t, \bar{z})$ along the dynamics of (4.57), we have

$$\begin{aligned} \dot{V}_0(t, \bar{z}) = \ & -\sum_{i=1}^{n-1} e_i^T e_i + e_{n-1}^T e_n - r^T e_{n-1} + r^T \left\{ Y\theta - \frac{y_s \theta_s}{\hat{y}_s \hat{\theta}_s} \left[\hat{Y}\hat{\theta} + K \mathrm{sat}\{\hat{r}\} \right] \right\} \\ & -\tilde{\theta}^T \Gamma^{-1} \dot{\hat{\theta}} - \tilde{\theta}_s^T \Gamma_s^{-1} \dot{\hat{\theta}}_s. \end{aligned} \tag{4.60}$$

By using the result in (4.8) and applying the parameter update laws defined in (4.56), (4.60) can be further upperbounded as follows

$$\begin{aligned} \dot{V}_0(t, \bar{z}) \leqslant \ & -\sum_{i=1}^{n-1} e_i^T e_i - r^T K r + r^T \left[\tilde{Y}\theta - \frac{\tilde{y}_s \theta_s}{\hat{y}_s \hat{\theta}_s} \left(\hat{Y}\hat{\theta} + K\hat{r} \right) \right] \\ & + \eta_n^T \left(K r + \hat{Y}\tilde{\theta} + \frac{\hat{y}_s \tilde{\theta}_s}{\hat{y}_s \hat{\theta}_s} \left(\hat{Y}\hat{\theta} + K\hat{r} \right) \right). \end{aligned} \tag{4.61}$$

In above inequality, the first two terms and last two terms in the right hand side can further simplified as follows

$$\dot{V}_0(t, \bar{z}) \leq -\lambda_3 \|z\|^2 + \delta_3 \|\eta\| \tag{4.62}$$

where $\lambda_3 \triangleq \min\{1, \lambda_{\min}(K)\}$ while δ_3 is a constant of analysis. In order to simplify the last two terms of (4.61), we have taken advantage of the following facts: (i) $Y(\cdot)\theta$ and $y_s(\cdot)\theta_s$

are locally Lipschitz in their arguments, (ii) the states are bounded inside the compact set $\mathcal{D}_c$, (iii) the state estimates are bounded via the sat$\{\cdot\}$ function; (iv) the parameter estimates are upperbounded via the update schemes given in (4.56), and (v) $\hat{y}_s\hat{\theta}_s$ is lowerbounded via projection as can be seen in (4.56). After adding the non-negative term $-\tilde{\theta}^T\tilde{\theta}-\tilde{\theta}_s^T\tilde{\theta}_s+\delta_0$ (see (4.47) and (4.55)) to the right-hand side of (4.62), and utilizing the uniform boundedness analysis given in (4.48), one can obtain

$$\dot{V}_0(t,\bar{z}) \leqslant -\lambda_3 \|\bar{z}\|^2 + \delta_0 + \delta_3 \|\eta\|. \tag{4.63}$$

From $W(\eta(t)) \leqslant \varrho\epsilon^2$ and results in (4.53), we know that $\|\eta(t)\| \leqslant \epsilon\sqrt{\varrho/\lambda_{\min}\{P_0\}}\ \forall \eta(t) \in \mathcal{D}_\epsilon$. Thus, (4.63) can be upperbounded as follows

$$\dot{V}_0(t,\bar{z}) \leqslant -\lambda_4 V_0 + \delta_0 + \delta_3\epsilon\sqrt{\varrho/\lambda_{\min}\{P_0\}} \tag{4.64}$$

where λ_4 has been defined previously in (4.55). At the boundary of the invariant set $\mathcal{D}_c$, two cases need to be considered: **Case 1***:* When $V_0(t,\bar{z}) = c > 2\delta_0/\lambda_4$, one can rewrite (4.64) as

$$\dot{V}_0(t,\bar{z}) \leqslant -\frac{\lambda_4}{2}V_0 + \delta_3\epsilon\sqrt{\varrho/\lambda_{\min}\{P_0\}}. \tag{4.65}$$

Define $\epsilon_1 \triangleq \dfrac{\lambda_4 c}{2\delta_3}\sqrt{\lambda_{\min}\{P_0\}/\varrho}$, then $\forall \epsilon \in (0,\ \epsilon_1]$ and $\eta(t) \in \mathcal{D}_\epsilon$, the following result holds on the boundary of $\mathcal{D}_c$

$$\dot{V}_0(t,\bar{z})\,|_{\partial\mathcal{D}_c, V_0=c} \leq 0. \tag{4.66}$$

Case 2*:* When $V_0(t,\bar{z}) < c$ and parameter errors $\tilde{\theta}$ and/or $\tilde{\theta}_s$ reach the boundary of the invariant set $\mathcal{D}_c$ as $\theta \in \partial\tilde{\Omega}_\theta$ and/or $\theta_s \in \partial\tilde{\Omega}_{\theta_s}$, the projection laws will guarantee $\theta(t)$ and/or $\theta_s(t)$ remaining inside the compact set $\mathcal{D}_c$. In the meantime, the variables not restricted by

projection will evolve freely until $V_0(t, \bar{z}) = c$ at which time Case 1 is applicable; thus, one can easily prove the invariance of the set $\mathcal{D}_c$ using (4.66). The derivative of $W(\eta)$ along the trajectory of (4.58) can be obtained as follows

$$\dot{W}(\eta) = \frac{\partial W(\eta)}{\partial \eta} \left(A_0 \eta(t)/\varepsilon + g(z(t), D_\eta \eta(t), t) \right). \tag{4.67}$$

By utilizing (4.53) as well as the fact that $P_0 A_0 + A_0^T P_0 = -I_{mn}$, $\dot{W}(\eta)$ can be upperbounded as

$$\dot{W}(\eta) \leqslant -\frac{1}{\epsilon} \|\eta\|^2 + 2 \|P_0\| \|\eta\| \|g\| \tag{4.68}$$

Based on (4.52), the aforementioned boundedness of the states and the parameter estimates, as well as the fact that ϵ is strictly less than 1, $\|g\|$ can be upperbounded as $\|g\| \leqslant \kappa_1 \|\eta\| + \kappa_2, \ \forall \ \bar{z}(t) \in \mathcal{D}_c$ and $\forall \ \eta(t) \in \mathbb{R}^{mn}$; here, $\kappa_1, \kappa_2 > 0$ are constants independent of ϵ. Utilization of this upperbound on $\|g\|$ in (4.68) allows us to formulate the following upperbound on $\dot{W}(\eta)$

$$\begin{aligned} \dot{W}(\eta) \leqslant \ & -\tfrac{1}{3\epsilon} \|\eta\|^2 - \|\eta\|^2 \left(\tfrac{1}{3\epsilon} - 2\kappa_1 \|P_0\| \right) \\ & - \|\eta\| \left(\tfrac{1}{3\epsilon} \|\eta\| - 2\kappa_2 \|P_0\| \right). \end{aligned} \tag{4.69}$$

Based on (4.53), $\|\eta\| \geqslant \epsilon \sqrt{\varrho / \|P_0\|}$ for $\eta(t) \in \partial \mathcal{D}_\epsilon$. If one chooses $\epsilon_2 < (6 \|P_0\| \kappa_1)^{-1}$, then $\forall \ \epsilon \in (0, \ \epsilon_2]$, a choice of $\varrho = 36 \kappa_2^2 \|P_0\|^3$ ensures that

$$\dot{W}(\eta)|_{\partial \mathcal{D}_\epsilon} \leqslant -\frac{1}{3\epsilon} \|\eta\|^2 \leqslant 0. \tag{4.70}$$

Thus, if one defines $\bar{\epsilon}_1 = \min\{1, \epsilon_1, \epsilon_2\}$, then (4.66) and (4.70) imply that $\Sigma = \mathcal{D}_c \times \mathcal{D}_\epsilon$ is an invariant set $\forall \epsilon \in (0, \bar{\epsilon}_1]$. ■

Theorem 2 *(**Boundedness Theorem**) There exists an $\bar{\epsilon}_2 \leqslant \bar{\epsilon}_1$ such that $\forall \epsilon \in (0, \bar{\epsilon}_2]$, any trajectory $(\bar{z}(t), \hat{z}(t))$ that starts inside $\mathcal{Z} \times \mathcal{H}$ is bounded for all time.*

Proof. Given the boundedness of $\bar{z}\,(0)$ and $\hat{z}\,(0)$, the definition of (4.50) implies that $\|\eta\,(0)\| \leqslant \kappa_6 \epsilon^{1-n}$ where κ_6 is a positive constant of analysis while n is the order of the system of (3.1). From the aforementioned boundedness assertions on $||f_r(z(t), \eta(t))||$, $\left\|\dot{\hat{\theta}}\right\|$, and $\left\|\dot{\hat{\theta}}_s\right\|$, it is easy to see that $\bar{z}\,(t)$ satisfies the following linear time growth upperbound in the compact set $\mathcal{D}_c$

$$\begin{aligned} \|\bar{z}\,(t) - \bar{z}(0)\| \leqslant & \ \|z(t) - z(0)\| + \left\|\tilde{\theta}\,(t) - \tilde{\theta}\,(0)\right\| \\ & + \left\|\tilde{\theta}_s\,(t) - \tilde{\theta}_s\,(0)\right\| \\ \leqslant & \ \kappa_3 t \end{aligned} \tag{4.71}$$

where κ_3 is a positive constant. Thus, there is a time T_c independent of ϵ such that $\bar{z}(t) \in \mathcal{D}_c, \ \forall \ t \in [0, T_c]$. Our aim now is to show that one can pick an ϵ such that if $\eta\,(t)$ starts outside the invariant set Σ, it can be made to enter the invariant set before $\bar{z}\,(t)$ can exit $\mathcal{D}_c$ – the key idea to be exploited here is the growth bound established in (4.71). Proving this previous assertion would imply that the solution $(\bar{z}\,(t), \eta\,(t))$ is in the invariant set Σ at some time T_ϵ which means that it will stay there $\forall \ t \in [T_\epsilon, \infty)$. Outside the invariant set, $W\,(\eta) \geqslant \varrho\epsilon^2 = 36\kappa_2^2 \left\|P_0\right\|^3 \epsilon^2$ which implies that $\|\eta\| \geqslant 6\epsilon\kappa_2 \left\|P_0\right\|$. From (4.53) and (4.70), one can upperbound $\dot{W}\,(\eta)$ as follows: $\dot{W}\,(\eta) \leqslant -\frac{1}{3\epsilon\|P_0\|} W\,(\eta)$. After solving the above inequality, an upperbound for $W\,(\eta)$ can be obtained as $W(\eta) \leqslant W\,(0) \exp(-\sigma_1 t/\epsilon)$, where $\sigma_1 \triangleq (3\left\|P_0\right\|)^{-1}$. Based on (4.53) and $\|\eta\,(0)\| \leqslant \kappa_6 \epsilon^{1-n}$, the upperbound on $W(\eta)$ can

be rewritten as follows

$$W(\eta) \leqslant \frac{\sigma_2}{\epsilon^{2(n-1)}} \exp(-\sigma_1 t/\epsilon) \tag{4.72}$$

where $\sigma_2 \triangleq \kappa_6^2 \|P_0\|$. Based on (4.72), we can find an $0 < \bar{\epsilon}_2 \leqslant \bar{\epsilon}_1$ small enough so that $W(\eta)$ enters $\mathcal{D}_\epsilon$ at a time $T_\epsilon \triangleq \frac{\epsilon}{\sigma_1} \ln\left(\frac{\sigma_2}{\varrho \epsilon^{2n}}\right) \leqslant T_c/2,\ \forall\ \epsilon \in (0, \bar{\epsilon}_2]$ where $\bar{\epsilon}_2 < \sqrt[2n]{\varrho^{-1}\sigma_2}/e$ – this upperbound on $\bar{\epsilon}_2$ is derived from the fact that T_ϵ is a monotonically increasing function only on $\epsilon \in (0,\ \sqrt[2n]{\varrho^{-1}\sigma_2}/e]$. Since $\eta(t)$ enters the invariant set $\mathcal{D}_\epsilon$ in less than half the time it takes for $\bar{z}(t)$ to exit $\mathcal{D}_c$, this implies that $(\bar{z}(t), \eta(t))$ enters Σ during $[0, T_\epsilon]$ and hence $\bar{z}(t), \eta(t) \in \mathcal{L}_\infty$ for all times $t \geqslant T_\epsilon$. Thus, $\forall\ t \in [0, T_\epsilon]$, the trajectory $(\bar{z}(t), \eta(t))$ is bounded by virtue of (4.71) and (4.72). Thus, we have proved that $(\bar{z}(t), \hat{z}(t))$ starting in $\mathcal{Z} \times \mathcal{H}$ are bounded for all time. ■

Theorem 3 *(**Ultimate Boundedness Theorem**) Given any solution $(\bar{z}(t), \hat{z}(t))$ that starts in $\mathcal{Z} \times \mathcal{H}$ and given any small $\delta > \sqrt{2(\lambda_1\lambda_4)^{-1}\delta_0}$, there exists an $0 < \bar{\epsilon}_3(\delta) \leqslant \bar{\epsilon}_2$ and a $T(\delta) > 0$ such that $\|\bar{z}(t)\| \leqslant \delta$ and $\|\hat{z}(t)\| \leqslant 2\delta,\ \forall\ t \geqslant T(\delta)$ and $\forall\ \epsilon \in (0, \bar{\epsilon}_3(\delta)]$.*

Proof. Inside the set Σ, (4.66) can be used to rewrite the upperbound on $\dot{V}_0(t, \bar{z})$ as

$$\begin{aligned} \dot{V}_0(t, \bar{z}) \leqslant\ & -\tfrac{\lambda_4}{2} V_0 \\ & -\tfrac{\lambda_4}{2}\left[V_0 - \tfrac{2}{\lambda_4}\left(\delta_0 + \delta_3 \epsilon \sqrt{\varrho/\lambda_{\min}\{P_0\}}\right)\right] \end{aligned} \tag{4.73}$$

Defining a compact set $\mathcal{D}_\mu \triangleq \left\{\bar{z} \in \mathbb{R}^{mn} \times \tilde{\Omega}_\theta\ \times \tilde{\Omega}_{\theta_s} |\ V_0 \leqslant c_\mu(\epsilon) = 2\lambda_4^{-1}\ \left(\delta_0 + \delta_3 \epsilon \sqrt{\varrho/\lambda_{\min}\{P_0\}}\right)\right\}$, then $\|\bar{z}(t)\| \notin \mathcal{D}_\mu$ implies that $\dot{V}_0(t, \bar{z})$ can be upperbounded as

$$\dot{V}_0(t, \bar{z}) \leqslant -\frac{\lambda_4}{2} V_0 < 0 \tag{4.74}$$

which shows that $V_0(t,\bar{z})$ is decreasing outside $\mathcal{D}_\mu$. Since it's always possible to find an $\epsilon_3 \in (0,\bar{\epsilon}_2]$ such that $2\delta_0/\lambda_4 < c_\mu(\epsilon_3) < c$, $\forall c > 2\delta_0/\lambda_4$, one can make $\mathcal{D}_\mu$ lie inside $\mathcal{D}_c$ by choosing ϵ small enough. From these assertions and the upperbound of (4.74), it is obvious that the set $\Sigma_{ub} \triangleq \mathcal{D}_\mu \times \mathcal{D}_\epsilon$ is positively invariant and $\mathcal{D}_\mu \subset \mathcal{D}_c$. According to the left inequality of (4.45), $V_0 \leqslant c_\mu(\epsilon)$ implies that $\lambda_1 \|\bar{z}\|^2 \leqslant c_\mu(\epsilon)$ which leads to $\|\bar{z}\| \leqslant \sqrt{\lambda_1^{-1} c_\mu(\epsilon)}$. Thus, given any $\delta = \sqrt{\lambda_1^{-1} c} > \sqrt{2(\lambda_1\lambda_4)^{-1}\delta_0}$, one can pick an $\epsilon_3 = \epsilon_3(\delta) \leqslant \bar{\epsilon}_2$ such that $\mathcal{D}_\mu \subset \mathcal{D}_\delta \triangleq \left\{\bar{z} \in \mathbb{R}^{mn} \times \tilde{\Omega}_\theta \times \tilde{\Omega}_{\theta_s} \mid \|\bar{z}(t)\| \leqslant \delta\right\}$. Moreover, any trajectory in Σ will enter Σ_{ub} in a finite time $T_{\epsilon 4} = T_{\epsilon 4}(\delta)$ $\forall \epsilon \in (0,\epsilon_3]$. Furthermore, from (4.72), $\lim_{\epsilon\to 0} W(\eta) = 0$, $\forall\ \epsilon \in (0,\bar{\epsilon}_2]$; hence, given any $\delta > \sqrt{2(\lambda_1\lambda_4)^{-1}\delta_0}$, we can find $\epsilon_4 = \epsilon_4(\delta) \leqslant \bar{\epsilon}_2$ such that $\forall\ \epsilon \in (0,\epsilon_4]$, we have $\|\eta(t)\| \leqslant \delta$, $\forall\ t \geqslant T_{\epsilon 4} \triangleq T_{\epsilon 4}(\delta)$. By defining $\bar{\epsilon}_3(\delta) \triangleq \min\{\epsilon_3(\delta),\ \epsilon_4(\delta)\}$ and $T(\delta) \triangleq \max\{T_{\epsilon 3}(\delta),\ T_{\epsilon 4}(\delta)\}$, we can obtain the following upperbound

$$\|\hat{z}(t)\| \leqslant \|\bar{z}(t)\| + \|\eta(t)\| \leqslant 2\delta$$

$$\forall \epsilon \in (0,\bar{\epsilon}_3(\delta)] \text{ and } \forall t \geqslant T(\delta).$$

Thus, one can conclude that $(\bar{z}(t), \hat{z}(t))$ starting in $\mathcal{Z} \times \mathcal{H}$ are ultimately bounded. It is also easy to see from above that the size of the ultimate bound for $\bar{z}(t)$ is determined by observer gain ϵ. As ϵ approaches zero, this ultimate bound δ will approach its lower bound $\sqrt{2(\lambda_1\lambda_4)^{-1}\delta_0}$ which is related to the amount of uncertainty in the parameters denoted by δ_0. ■

In the simulation, the model given in (4.37) has been considered with the same parameters and initial conditions. The control gain K in (4.54) have been chosen as $diag\{7.5, 4.5\}$

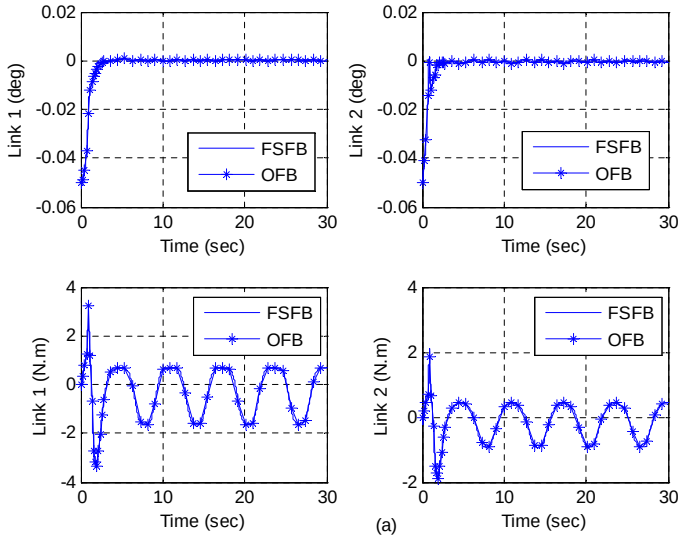

Figure 4.7: Tracking Error and Control Input Comparison between FSFB and OFB.

through trial and error method. In (4.56), the gains for the adaptation law (4.56) are chosen as $\Gamma = 30I_9$ and $\Gamma_{laos} = 75I_3$. The parameters estimates were initialized as $\hat{\theta}(0) =$ [4.32, 1.07, 1.14, 0.54, 4.18, 0.65, 0.88, 1.18, 0.40], $\hat{\theta}_s(0) = \begin{bmatrix} 2.88 & 0.80 & 1.35 \end{bmatrix}$. The projection boundaries for above parameters are set as ± 10. The parameters for HGO defined in (4.34) are selected as $a_1 = 0.91$, $a_2 = 0.15$, and $\varepsilon = 0.0005$ by trial and error. The saturation bound for $\hat{z}(t)$ is set at ± 100. Fig. 4.7 shows the tracking errors under FSFB and OFB and the corresponding control inputs while Fig. 4.8 shows the parameter estimation results.

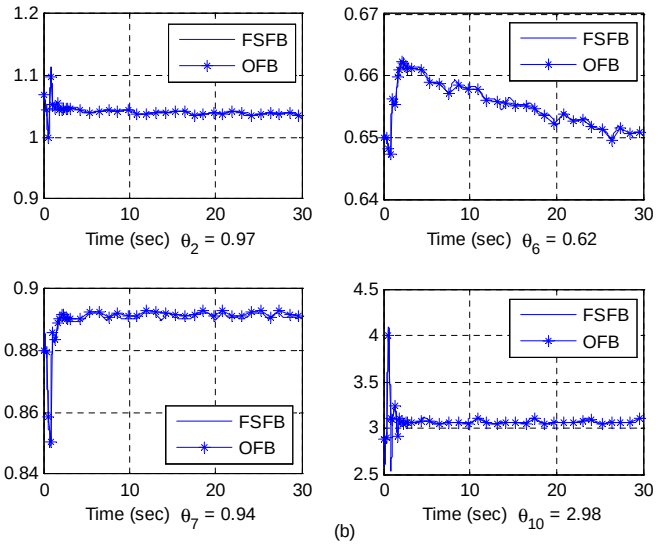

Figure 4.8: Sample of Parameter Estimation Comparison between FSFB and OFB.

4.3 Model-Free MIMO Nonlinear Control Design for an Aeroelastic System

A 2-DOF pitch-plunge wing section with both LECS and TECS is shown in Fig. 4.9 where both leading and trailing edge control surfaces are used as control inputs. The aeroelastic governing equation subject to external disturbance is developed from previous models:

$$\begin{bmatrix} m_T & m_w x_\alpha b \\ m_w x_\alpha b & I_\alpha \end{bmatrix} \begin{bmatrix} \ddot{h} \\ \ddot{\alpha} \end{bmatrix} + \begin{bmatrix} c_h & 0 \\ 0 & c_\alpha \end{bmatrix} \begin{bmatrix} \dot{h} \\ \dot{\alpha} \end{bmatrix} + \begin{bmatrix} k_h & 0 \\ 0 & k_\alpha(\alpha) \end{bmatrix} \begin{bmatrix} h \\ \alpha \end{bmatrix} = \begin{bmatrix} -L - L_g \\ M + M_g \end{bmatrix}. \tag{4.75}$$

The definition of symbols used in above equation can be found in [30]. In (4.75), the

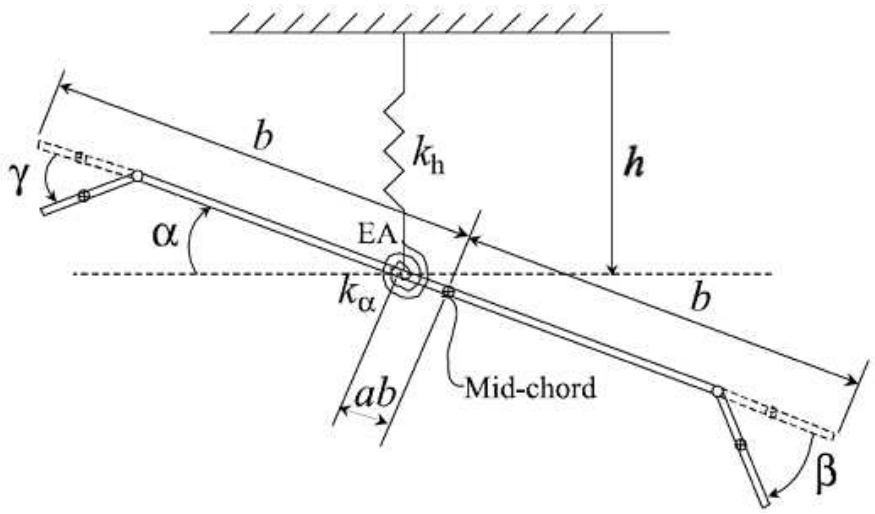

Figure 4.9: Two DOF aeroelastic system with both leading- and trailing-edge control surfaces.

quasi-steady lift $L(\dot{h}, \dot{\alpha}, h, \alpha, \beta, \gamma)$ and aerodynamic moment $M(\dot{h}, \dot{\alpha}, h, \alpha, \beta, \gamma)$ are given as

$$\begin{aligned} L &= \rho U_\infty^2 bsC_{l\alpha}(\alpha + \tfrac{\dot{h}}{U_\infty} + (\tfrac{1}{2} - a)b\tfrac{\dot{\alpha}}{U_\infty}) + \rho U_\infty^2 bsC_{l\beta}\beta + \rho U_\infty^2 bsC_{l\gamma}\gamma, \\ M &= \rho U_\infty^2 b^2 sC_{m\alpha-eff}(\alpha + \tfrac{\dot{h}}{U_\infty} + (\tfrac{1}{2} - a)b\tfrac{\dot{\alpha}}{U_\infty}) + \rho U_\infty^2 b^2 sC_{m\beta-eff}\beta + \rho U_\infty^2 b^2 sC_{m\gamma-eff}\gamma \end{aligned} \tag{4.76}$$

where $C_{m\alpha-eff}$, $C_{m\beta-eff}$, and $C_{m\gamma-eff}$ are defined as follows

$$\begin{aligned} C_{m\alpha-eff} &= (\tfrac{1}{2} + a)C_{l\alpha} + 2C_{m\alpha}, \\ C_{m\beta-eff} &= (\tfrac{1}{2} + a)C_{l\beta} + 2C_{m\beta}, \\ C_{m\gamma-eff} &= (\tfrac{1}{2} + a)C_{l\gamma} + 2C_{m\gamma}. \end{aligned} \tag{4.77}$$

The aerodynamic loads due to the bounded external disturbance can be given as [43]

$$\begin{aligned} L_g &= \rho U_\infty^2 bsC_{l\alpha} w_G(\tau)/U_\infty = \rho U_\infty bsC_{l\alpha} w_G(\tau), \\ M_g &= \left(\tfrac{1}{2} - a\right) bL_g \end{aligned} \tag{4.78}$$

where $w_G(\tau)$ denotes the disturbance velocity while τ is a dimensionless time variable defined as $\tau = U_\infty t/b$. Motivated by [20], the governing equations (4.75) can be transformed using (4.76) into the following input-output representation that is amenable to model-free output feedback design

$$\ddot{\mathbf{x}} = \mathbf{h}(\mathbf{x}, \dot{\mathbf{x}}) + \mathbf{w}_{hd} + \mathbf{G}_s \mathbf{u} \tag{4.79}$$

where $\mathbf{x} \triangleq [h,\ \alpha]^T \in \Re^2$ is a vector of system output, $\mathbf{u} = [u_1,\ u_2]^T \triangleq [\beta,\ \gamma]^T \in \Re^2$ denotes the control input vector, $\mathbf{h}(\mathbf{x}, \dot{\mathbf{x}})$ contains uncertain nonlinearities due to the existence of $k_\alpha(\alpha)$, while $\mathbf{w}_{hd}$ represents bounded unknown external disturbance terms. Here, $\mathbf{G}_s \triangleq \begin{bmatrix} g_{11} & g_{12} \\ g_{21} & g_{22} \end{bmatrix} \in \Re^{2\times 2}$ is a constant non-singular gain matrix for which the constant matrix

entries g_{ij} are explicitly defined as follows

$$\begin{aligned} g_{11} &= -U_\infty^2 \Delta^{-1} \rho b s \left(I_\alpha C_{l\beta} + m_w x_\alpha b^2 C_{m\beta-eff} \right), \\ g_{12} &= -U_\infty^2 \Delta^{-1} \rho b s \left(I_\alpha C_{l\gamma} + m_w x_\alpha b^2 C_{m\gamma-eff} \right), \\ g_{21} &= U_\infty^2 \Delta^{-1} \rho b s \left(m_w x_\alpha b C_{l\beta} + m_T b C_{m\beta-eff} \right), \\ g_{22} &= U_\infty^2 \Delta^{-1} \rho b s \left(m_w x_\alpha b C_{l\gamma} + m_T b C_{m\gamma-eff} \right), \end{aligned} \tag{4.80}$$

where $\Delta \triangleq \det(\mathbf{G}_s) = m_T I_\alpha - m_w^2 x_\alpha^2 b^2 \neq 0$. Based on the matrix decomposition introduced in [1] and the facts that both the leading principal minors g_{11} and Δ are non-zero, $\mathbf{G}_s$ can be decomposed as $\mathbf{G}_s = \mathbf{SDU}$ where $\mathbf{S}$ is a symmetric, positive-definite matrix, $\mathbf{D}$ is a diagonal matrix with diagonal entries $+1$ or -1, and $\mathbf{U}$ is an unknown unity upper triangular matrix. This $\mathbf{SDU}$ decomposition is a key factor in the proposed algebraic-loop free controller design. According to the $\mathbf{SDU}$ decomposition result previously obtained in [44], $\mathbf{S}$, $\mathbf{D}$, and $\mathbf{U}$ can be explicitly written as

$$\mathbf{S} = \begin{bmatrix} |g_{11}| & \text{sign}(g_{11}) g_{21} \\ \text{sign}(g_{11}) g_{21} & \text{sign}(g_{11}) \text{sign}(\Delta) [g_{22} - g_{11}^{-1} g_{21} (g_{12} - g_{21} \text{sign}(\Delta))] \end{bmatrix},$$

$$\mathbf{D} = \begin{bmatrix} \text{sign}(g_{11}) & 0 \\ 0 & \text{sign}(g_{11}) \text{sign}(\Delta) \end{bmatrix}, \quad \mathbf{U} = \begin{bmatrix} 1 & \dfrac{|g_{11}^{-1}| (g_{12} - g_{21} \text{sign}(\Delta))}{\text{sign}(g_{11})} \\ 0 & 1 \end{bmatrix} \tag{4.81}$$

where the notation $\text{sign}(\cdot)$ denotes the standard signum function. For purposes of control design, we assume that the signs of the leading principal minors of the high-frequency gain matrix $\mathbf{G}_s$ are known, i.e., the diagonal matrix $\mathbf{D}$ is assumed to be known. After applying the matrix decomposition property and multiplying both sides of (4.79) with $\mathbf{T} \triangleq \mathbf{S}^{-1} \in \Re^{2\times 2}$,

(4.79) can be rewritten as

$$\mathbf{T}\ddot{\mathbf{x}} = \mathbf{f}\left(\mathbf{x}, \dot{\mathbf{x}}\right) + \mathbf{w}_d + \mathbf{DUu} \tag{4.82}$$

where $\mathbf{T}$ is a symmetric, positive definite matrix, $\mathbf{f}\left(\mathbf{x}, \dot{\mathbf{x}}\right) \triangleq \mathbf{S}^{-1}\mathbf{h}\left(\mathbf{x}, \dot{\mathbf{x}}\right) \in \Re^2$ contains unmodeled nonlinearities, while $\mathbf{w}_d \triangleq \mathbf{S}^{-1}\mathbf{w}_{hd} \in \Re^2$ represents a bounded unknown external disturbance term.

The tracking error $\mathbf{e}_1(t) \in \Re^2$ for the aeroelastic system can be defined as $\mathbf{e}_1 \triangleq \mathbf{x}_d - \mathbf{x}$. Here, $\mathbf{x}_d \in \Re^2$ is the desired output vector that is designed to be $\mathcal{C}^2$ smooth in deference to the requirements of the subsequent control design. Since the control objective is to suppress the aeroelastic vibrations, one can simply choose $\mathbf{x}_d$ to be zero all the time or use another desirable smooth trajectory $\mathbf{x}_d$ along which the actual pitching and plunging variables encoded by $\mathbf{x}$ can be driven toward the origin (by virtue of the subsequent control design). Next, to simplify the subsequent control design, the auxiliary error signals $\mathbf{e}_2\left(t\right) \in \Re^2$ and filtered tracking error $\mathbf{r}\left(t\right) \in \Re^2$ are introduced as follows

$$\mathbf{e}_2 = \dot{\mathbf{e}}_1 + \mathbf{e}_1, \qquad \mathbf{r} = \mathbf{e}_2 + \mathbf{e}_1. \tag{4.83}$$

Then, based on above definitions, a composite error signal can be defined as follows

$$\mathbf{z} \triangleq \left[\mathbf{e}_1^T,\ \mathbf{e}_2^T,\ \mathbf{r}^T\right]^T.$$

By taking the time derivative of $\mathbf{r}$ and substituting from the derivative of $\mathbf{e}_2$, one can easily obtain the following relation

$$\dot{\mathbf{r}} = \ddot{\mathbf{e}}_2 + 2\dot{\mathbf{e}}_1. \tag{4.84}$$

After premultiplying both sides of (4.84) by $\mathbf{T}$ and applying the definitions given in (4.82) and (4.83), (4.84) can be rewritten as

$$\mathbf{T}\dot{\mathbf{r}} = \mathbf{T}\left(\ddot{\mathbf{x}}_d + 2\dot{\mathbf{e}}_1\right) - \mathbf{f}\left(\mathbf{x}, \dot{\mathbf{x}}\right) - \mathbf{w}_d - \mathbf{D}\mathbf{U}\mathbf{u}. \tag{4.85}$$

Furthermore, given a strictly upper triangular matrix $\bar{\mathbf{U}} = \mathbf{D}\mathbf{U} - \mathbf{D}$, the open-loop dynamics of (4.85) can be rewritten as follows

$$\mathbf{T}\dot{\mathbf{r}} = \mathbf{T}\left(\ddot{\mathbf{x}}_d + 2\dot{\mathbf{e}}_1\right) - \mathbf{f}\left(\mathbf{x}, \dot{\mathbf{x}}\right) - \mathbf{w}_d - \bar{\mathbf{U}}\mathbf{u} - \mathbf{D}\mathbf{u}. \tag{4.86}$$

Assumed that both the output vector $\mathbf{x}$ and their first order time derivative $\dot{\mathbf{x}}$ can be measured directly. As previously stated, $\mathbf{f}\left(\mathbf{x}, \dot{\mathbf{x}}\right)$ denotes unmodeled system nonlinearities while $\mathbf{w}_d$ represents a bounded unknown external disturbance term. Furthermore, $\mathbf{T}$ and $\bar{\mathbf{U}}$ are assumed to be unknown while the diagonal matrix $\mathbf{D}$ comprising the signs of the leading principal minors of $\mathbf{G}_s$ is assumed to be known. Given these assumptions, the following full-state feedback control law is proposed

$$\mathbf{u} = \mathbf{D}^{-1}\left[\mathbf{K}\mathbf{r} + \hat{\mathbf{N}} - \mathbf{v}\right] \tag{4.87}$$

where $\mathbf{K} = \mathbf{K}_v + \mathbf{K}_d + \mathbf{K}_\lambda$ with $\mathbf{K}_v = k_v\mathbf{I}_{2\times 2},\ \mathbf{K}_d = k_d\mathbf{I}_{2\times 2},\ \mathbf{K}_\lambda = diag\left\{k_{\Lambda_1},\ 0\right\}$ while $\hat{\mathbf{N}}$ and $\mathbf{v}$ represent the feedforward compensator and robustifying term, respectively, to be designed later. After substituting (4.87) into the open-loop dynamics of (4.86) and rearranging some terms, one can obtain the following closed-loop dynamics

$$\begin{aligned} \mathbf{T}\dot{\mathbf{r}} = \ & -\mathbf{K}_d\mathbf{e}_2 + \mathbf{T}\left(\ddot{\mathbf{x}}_d + 2\dot{\mathbf{e}}_1\right) - \mathbf{f}\left(\mathbf{x}, \dot{\mathbf{x}}\right) + \mathbf{K}_d\mathbf{e}_2 \\ & -\mathbf{w}_d - \bar{\mathbf{U}}\mathbf{u} - \left(\mathbf{K}_v + \mathbf{K}_d + \mathbf{K}_\lambda\right)\mathbf{r} - \hat{\mathbf{N}} + \mathbf{v} \end{aligned} \tag{4.88}$$

where $\mathbf{K}_d\mathbf{e}_2$ has been added and subtracted in the above equation. In the above open-loop dynamics, $\mathbf{T}\left(\ddot{\mathbf{x}}_d + 2\dot{\mathbf{e}}_1\right)$, $\mathbf{f}\left(\mathbf{x}, \dot{\mathbf{x}}\right)$, $\bar{\mathbf{U}}\mathbf{u}$, and $\mathbf{w}_d$ represent unknown system model and external disturbance as previously stated. These terms will be dealt with by utilizing nonlinear damping and feedforward compensation. To facilitate further development, one can define the auxiliary signals Λ and Φ as follows

$$\begin{aligned} \Lambda &= d_2^{-1}\bar{U}_{12}K_{22}r_2 = \rho_\Lambda r_2, \\ \Phi &= d_2^{-1}\bar{U}_{12}\left(\hat{N}_2 - v_2\right) \end{aligned} \tag{4.89}$$

where d_i denotes the i^{th} diagonal element of $\mathbf{D}^{-1}$**,** K_{ij} and $\bar{U}_{ij}$ represent the ij^{th} element of the matrices $\mathbf{K}$ and $\bar{\mathbf{U}}$, respectively, while $\rho_\Lambda \triangleq d_2^{-1}\bar{U}_{12}K_{22}$ is an unknown constant scalar since $\bar{\mathbf{U}}$ is unknown. Based on the control input defined in (4.87) and the definitions given in (4.89), the vector $\bar{\mathbf{U}}\mathbf{u}$ in (4.88) can be written as follows

$$\bar{\mathbf{U}}\mathbf{u} = \left[\bar{U}_{12}u_2,\ 0\right]^T = \left[\Lambda + \Phi,\ 0\right]^T \tag{4.90}$$

where u_i denotes the i^{th} element of the control input vector $\mathbf{u}$. By employing (4.90) and rearranging some terms, the closed-loop dynamics of (4.88) can be rewritten as follows

$$\begin{aligned} \mathbf{T}\dot{\mathbf{r}} = \ & -\mathbf{K}_d\mathbf{e}_2 - \left(\mathbf{K}_d + \mathbf{K}_\lambda\right)\mathbf{r} - \left[\Lambda,\ 0\right]^T - \mathbf{K}_v\mathbf{r} + \mathbf{T}\left(\ddot{\mathbf{x}}_d + 2\dot{\mathbf{e}}_1\right) \\ & -\mathbf{f}\left(\mathbf{x}, \dot{\mathbf{x}}\right) + \mathbf{K}_d\mathbf{e}_2 - \begin{bmatrix} \Phi, & 0 \end{bmatrix}^T - \hat{\mathbf{N}} - \mathbf{w}_d + \mathbf{v}. \end{aligned} \tag{4.91}$$

Given the expression of (4.91), a nonlinear target function $\mathbf{N} \in \Re^2$, which contains the unknown system vectors $\mathbf{T}\left(\cdot\right)$ and $\mathbf{f}\left(\cdot\right)$, can be defined as follows

$$\mathbf{N}\left(\bar{\mathbf{x}}_\mathbf{t}\right) = \mathbf{T}\left(\ddot{\mathbf{x}}_d + 2\dot{\mathbf{e}}_1\right) - \mathbf{f}\left(\mathbf{x}, \dot{\mathbf{x}}\right) + \mathbf{K}_d\mathbf{e}_2 - \begin{bmatrix} \Phi, & 0 \end{bmatrix}^T. \tag{4.92}$$

Here, the input vector $\bar{\mathbf{x}}_t \in \Re^{\mathbf{11}}$ for the nonlinear target function can be defined as follows

$$\bar{\mathbf{x}}_t = \left[\mathbf{x}^T,\ \dot{\mathbf{x}}^{\mathbf{T}},\ \mathbf{x}_d^T,\ \dot{\mathbf{x}}_d^T,\ \ddot{\mathbf{x}}_d^T,\ \left\|\hat{\mathbf{Z}}\right\|_F\right]^T \tag{4.93}$$

where $\|\cdot\|_F$ denotes the Frobenius norm and $\hat{\mathbf{Z}}$ is a composite weight matrix estimate which will be subsequently designed. A feedforward compensator $\hat{\mathbf{N}}$ will be designed to compensate this nonlinear target function $\mathbf{N}$ which contains the unknown system model. In order to facilitate the stability analysis, $\mathbf{\Pi}$ and $\mathbf{\Psi}$ can be defined by using the definitions in (4.89) and (4.92) as follows

$$\mathbf{\Pi} = -\left[\Lambda,\ 0\right]^T, \qquad \mathbf{\Psi} = -\mathbf{K}_v\mathbf{r} + \mathbf{N} - \hat{\mathbf{N}} - \mathbf{w}_d + \mathbf{v}. \tag{4.94}$$

After employing (4.92) and (4.94), one can finally rewrite the closed-loop dynamics of (4.91) as

$$\mathbf{T}\dot{\mathbf{r}} = -\mathbf{K}_d\mathbf{e}_2 - \left(\mathbf{K}_d + \mathbf{K}_\lambda\right)\mathbf{r} + \mathbf{\Pi} + \mathbf{\Psi}. \tag{4.95}$$

It will be subsequently shown how the unknown term $\mathbf{\Pi}$ can be nonlinearly damped out by the feedback control term $\left(\mathbf{K}_d + \mathbf{K}_\lambda\right)\mathbf{r}$ and how the feedforward compensator $\hat{\mathbf{N}}$ and robustifying term $\mathbf{v}$ can be designed in order to compensate for the unknown terms $\mathbf{T}\left(\ddot{\mathbf{x}}_d + 2\dot{\mathbf{e}}_1\right)$, $\mathbf{f}\left(\mathbf{x}, \dot{\mathbf{x}}\right)$, and $\begin{bmatrix} \Phi, & 0 \end{bmatrix}^T$.

Since the model of the wing section and external disturbance are assumed to be unknown in the control design, adaptive control designs cannot be applied. In lieu of adaptation, a neural network feedforward compensator $\hat{\mathbf{N}}$ along with robustifying term $\mathbf{v}$ are proposed to compensate for this target function $\mathbf{N}$ and the disturbance signal $\mathbf{w}_d$ – thus, model-free con-

trol design is facilitated by exploiting the twin neural properties of universal approximation and online (i.e., real-time) learning.

The nonlinear target function $\mathbf{N}$ defined in (4.92) can be approximated as a three-layer neural network target function of the form [45]

$$\mathbf{N}\left(\bar{\mathbf{x}}\right) = \mathbf{W}^T \boldsymbol{\sigma}\left(\mathbf{V}^T \bar{\mathbf{x}}\right) + \boldsymbol{\epsilon}\left(\bar{\mathbf{x}}\right) \tag{4.96}$$

where $\bar{\mathbf{x}} = \begin{bmatrix} 1, & \bar{\mathbf{x}}_t^T \end{bmatrix}^T \in \Re^{p_1+1}$ denotes the augmented input vector while $\boldsymbol{\sigma}\left(\cdot\right) \in \Re^{p_2+1}$ denotes the activation function - in this approach, a sigmoid function is chosen as the activation function. $\boldsymbol{\epsilon}\left(\bar{\mathbf{x}}\right) \in \Re^{p_3}$ is the functional reconstruction error vector, $\mathbf{V} \in \Re^{(p_1+1)\times p_2}$ is the ideal first layer interconnection weight matrix between input layer and hidden layer, $\mathbf{W} \in \Re^{(p_2+1)\times p_3}$ denotes the ideal second layer interconnection weight matrix between hidden layer and output layer, while $p_1 + 1$, $p_2 + 1$, and p_3 are the number of nodes in the input layer, hidden layer, and output layer, respectively. Note that the input vector $\bar{\mathbf{x}}$ and $\boldsymbol{\sigma}\left(\cdot\right)$ are augmented vectors because of placement of '1' as their first element since thresholds are included as the first columns of the weight matrices $\mathbf{W}$ and $\mathbf{V}$. For the problem at hand, it will be assumed that the ideal weight matrices $\mathbf{W}$ and $\mathbf{V}$ are constant and bounded such that $\left\|\mathbf{W}\right\|_F \leq \mathbf{W}_B$ and $\left\|\mathbf{V}\right\|_F \leq \mathbf{V}_B$, where $\mathbf{W}_B$ and $\mathbf{V}_B$ are positive constants and $\left\|\cdot\right\|_F$ denotes the Frobenius norm. The approximation error is assumed to be bounded in a compact set by $\left\|\boldsymbol{\epsilon}\left(\bar{\mathbf{x}}\right)\right\| < \epsilon_N$ where ϵ_N is an unknown positive constant related to the number of nodes in the hidden layer. Based on (4.96), the typical three-level neural network compensator for

target function $\mathbf{N}(\bar{\mathbf{x}})$ is given in the following form

$$\hat{\mathbf{N}}(\bar{\mathbf{x}}) = \hat{\mathbf{W}}^T \boldsymbol{\sigma}\left(\hat{\mathbf{V}}^T \bar{\mathbf{x}}\right) \tag{4.97}$$

where $\hat{\mathbf{W}}$ and $\hat{\mathbf{V}}$ are estimated weight matrices. Here $\hat{\mathbf{W}}$ and $\hat{\mathbf{V}}$ can be set to zero at first or randomly initialized within certain region, which implies that there is no requirement for preliminary off-line learning phase for the neural network. Motivated by [45] and the ensuing stability analysis, the estimated weight matrices can be updated or learned through on-line weight tuning algorithms of the form

$$\begin{aligned} \dot{\hat{\mathbf{W}}} = & \left(\mathbf{F}\hat{\boldsymbol{\sigma}} - \mathbf{F}\hat{\boldsymbol{\sigma}}'\hat{\mathbf{V}}^T\bar{\mathbf{x}}\right)\mathbf{r}^T - \kappa\mathbf{F}\|\mathbf{r}\|\hat{\mathbf{W}}, \\ \dot{\hat{\mathbf{V}}} = & \mathbf{G}\bar{\mathbf{x}}\left(\hat{\boldsymbol{\sigma}}'^T\hat{\mathbf{W}}\mathbf{r}^T\right)^T - \kappa\mathbf{G}\|\mathbf{r}\|\hat{\mathbf{V}} \end{aligned} \tag{4.98}$$

where $\mathbf{F} \in \Re^{(p_2+1)\times(p_2+1)}$ and $\mathbf{G} \in \Re^{(p_1+1)\times(p_1+1)}$ are positive-definite, diagonal gain matrices, $\kappa > 0$ is a scalar design parameter, $\hat{\boldsymbol{\sigma}} = \boldsymbol{\sigma}\left(\hat{\mathbf{V}}^T\bar{\mathbf{x}}\right)$ and $\hat{\boldsymbol{\sigma}}' \equiv d\boldsymbol{\sigma}\left(\hat{\mathbf{V}}^T\bar{\mathbf{x}}\right)/d\left(\hat{\mathbf{V}}^T\bar{\mathbf{x}}\right)$. After substituting (4.96) and (4.97) into (4.94) and applying a Taylor series expansion, $\boldsymbol{\Psi}$ defined in (4.94) can be given as

$$\boldsymbol{\Psi} = -\mathbf{K}_v\mathbf{r} + \tilde{\mathbf{W}}^T\left[\hat{\boldsymbol{\sigma}} - \hat{\boldsymbol{\sigma}}'\hat{\mathbf{V}}^T\bar{\mathbf{x}}\right] + \hat{\mathbf{W}}^T\hat{\boldsymbol{\sigma}}'\tilde{\mathbf{V}}^T\bar{\mathbf{x}} + \mathbf{w} + v \tag{4.99}$$

where $\tilde{\mathbf{W}} = \mathbf{W} - \hat{\mathbf{W}}$ and $\tilde{\mathbf{V}} = \mathbf{V} - \hat{\mathbf{V}}$ denote weight matrices estimation errors while $\mathbf{w}$ can be written as

$$\mathbf{w} = \tilde{\mathbf{W}}^T\hat{\boldsymbol{\sigma}}'\mathbf{V}^T\bar{\mathbf{x}} + \tilde{\mathbf{W}}^T O\left(\tilde{\mathbf{V}}^T\bar{\mathbf{x}}\right)^2 + \epsilon(\bar{\mathbf{x}}) - \mathbf{w}_d. \tag{4.100}$$

To facilitate the subsequent analysis, one can also obtain a compact form representation for $\|\mathbf{w}\|$ as follows

$$\|\mathbf{w}\| \quad = C_0 + C_1\left\|\tilde{\mathbf{Z}}\right\|_F + C_2\left\|\tilde{\mathbf{Z}}\right\|_F\|\mathbf{r}\| \tag{4.101}$$

where C_0, C_1, and C_2 are all positive constants while the ideal composite weight matrix $\mathbf{Z}$, estimated composite weight matrix $\hat{\mathbf{Z}}$, and the composite weight mismatch matrix $\tilde{\mathbf{Z}}$ are defined as follows

$$\mathbf{Z} = \begin{bmatrix} \mathbf{W} & \mathbf{0} \\ \mathbf{0} & \mathbf{V} \end{bmatrix}, \quad \hat{\mathbf{Z}} \equiv \begin{bmatrix} \hat{\mathbf{W}} & \mathbf{0} \\ \mathbf{0} & \hat{\mathbf{V}} \end{bmatrix}, \quad \tilde{\mathbf{Z}} \equiv \begin{bmatrix} \tilde{\mathbf{W}} & \mathbf{0} \\ \mathbf{0} & \tilde{\mathbf{V}} \end{bmatrix} \tag{4.102}$$

where $\tilde{\mathbf{Z}} = \mathbf{Z} - \hat{\mathbf{Z}}$. According to the boundedness property for $\|\mathbf{W}\|_F$ and $\|\mathbf{V}\|_F$, it's assumed that there exists a constant Z_B such that $Z_B > \|\mathbf{Z}\|_F$. Based on the definition of Z_B, the robustifying term $\mathbf{v}$ in (4.87) can be defined as

$$\mathbf{v} = -K_z \left(\left\| \hat{\mathbf{Z}} \right\|_F + Z_B \right) \mathbf{r} \tag{4.103}$$

where K_z is a positive constant. Finally, it is noted that the unknown external disturbance $\mathbf{w}_d$ and functional reconstruction error $\epsilon(\bar{\mathbf{x}})$ are assumed to be bounded.

The stability analysis for the proposed model-free controller is provided in the following theorem. In order to facilitate ease of expression, the stability analysis is split into two parts which comprise components of the derivative of the Lyapunov function. While the first part shows the usefulness of the nonlinear damping technique, the second part shows the utility of the feedforward compensator and the robustifying injection term in proving system stability. A Uniformly Ultimately Bounded (UUB) result is obtained for both the norm of the filtered tracking error $\mathbf{r}$ and the norm of the neural network weight estimation error $\tilde{\mathbf{Z}}$**.** Note a signal is uniformly ultimately bounded [36] if there exist positive constants b and c, independent of $t_0 \geq 0$, and for every $a \in (0, c)$, there is $T = T(a, b) \geq 0$, independent of t_0, such that

$$\|x(t_0)\| \leq a \Rightarrow \|x(t)\| \leq b, \ \forall t \geq t_0 + T.$$

Theorem 4 *Provided the control gain matrix* $\mathbf{K}$ *defined in (4.87) is chosen to be appropriately large, the error signals (*$\mathbf{r}$ *and* $\tilde{\mathbf{Z}}$*) for the closed-loop system defined in (4.95) are Uniformly Ultimately Bounded (UUB).*

Proof. Firstly, a non-negative Lyapunov function candidate V_0 is defined as

$$V_0 = \frac{1}{2}\mathbf{e}_1^T\mathbf{K}_d\mathbf{e}_1 + \frac{1}{2}\mathbf{r}^T\mathbf{T}\mathbf{r} + \frac{1}{2}tr\left\{\tilde{\mathbf{W}}^T\mathbf{F}^{-1}\tilde{\mathbf{W}}\right\} + \frac{1}{2}tr\left\{\tilde{\mathbf{V}}^T\mathbf{G}^{-1}\tilde{\mathbf{V}}\right\}. \tag{4.104}$$

After differentiating (4.104) and using the results obtained in (4.95) and (4.99), the following expressions are obtained

$$\dot{V}_0 = \dot{V}_1 + \dot{V}_2 \tag{4.105}$$

where

$$\begin{aligned} \dot{V}_1 &= \mathbf{e}_1^T\mathbf{K}_d\dot{\mathbf{e}}_1 - \mathbf{r}^T\mathbf{K}_d\mathbf{e}_2 + \mathbf{r}^T\left[-\left(\mathbf{K}_d + \mathbf{K}_\lambda\right)\mathbf{r} + \mathbf{\Pi}\right], \\ \dot{V}_2 &= \mathbf{r}^T\mathbf{\Psi} + tr\left\{\tilde{\mathbf{W}}^T\mathbf{F}^{-1}\dot{\tilde{\mathbf{W}}}\right\} + tr\left\{\tilde{\mathbf{V}}^T\mathbf{G}^{-1}\dot{\tilde{\mathbf{V}}}\right\}. \end{aligned} \tag{4.106}$$

After utilizing the error definitions of (4.83), one can obtain the following expression for $\dot{V}_1$

$$\dot{V}_1 = -\mathbf{e}_1^T\mathbf{K}_d\mathbf{e}_1 - \mathbf{e}_2^T\mathbf{K}_d\mathbf{e}_2 - \mathbf{r}^T\mathbf{K}_d\mathbf{r} - \mathbf{r}^T\mathbf{K}_\lambda\mathbf{r} + \mathbf{r}^T\mathbf{\Pi} \tag{4.107}$$

which can be upperbounded by employing the definitions of $\mathbf{z}$, $\mathbf{\Pi}$, Λ, k_{Λ_1}, and k_d as follows

$$\dot{V}_1 \leq -k_d\left\|\mathbf{z}\right\|^2 + \left[\left\|\rho_\Lambda\right\|\left\|\mathbf{z}\right\|\left\|\mathbf{r}_1\right\| - k_{\Lambda_1}\left\|\mathbf{r}_1\right\|^2\right] \tag{4.108}$$

where (4.89) has been utilized to obtain the fact that $\left\|\Lambda\right\| < \left\|\rho_\Lambda\right\|\left\|\mathbf{z}\right\|$. After completing the squares on the bracketed term in (4.108), the following upperbound is obtained

$$\dot{V}_1 \leq -\left(k_d - \frac{\left\|\rho_\Lambda\right\|^2}{4k_{\Lambda_1}}\right)\left\|\mathbf{z}\right\|^2. \tag{4.109}$$

By choosing k_d and k_{Λ_1} large enough such that bracketed term in (4.109) is positive, one can easily see that $\dot{V}_1$ in (4.105) can be upper bounded as follows

$$\dot{V}_1 \leq -\gamma\left(\|\mathbf{z}\|^2\right) \tag{4.110}$$

where $\gamma\left(\|\mathbf{z}\|^2\right)$ is a class $\mathcal{K}_\infty$ function. Next, by substituting the expression for $\mathbf{\Psi}$ given in (4.99), $\dot{V}_2$ can be obtained as follows

$$\begin{aligned}\dot{V}_2 = \ & \mathbf{r}^T\left[-\mathbf{K}_v\mathbf{r} + \tilde{\mathbf{W}}^T\left[\hat{\boldsymbol{\sigma}} - \hat{\boldsymbol{\sigma}}'\hat{\mathbf{V}}^T\bar{\mathbf{x}}\right] + \hat{\mathbf{W}}^T\hat{\boldsymbol{\sigma}}'\tilde{\mathbf{V}}^T\bar{\mathbf{x}} + \mathbf{w} + \mathbf{v}\right] \\ & + tr\left\{\tilde{\mathbf{W}}^T\mathbf{F}^{-1}\dot{\tilde{\mathbf{W}}}\right\} + tr\left\{\tilde{\mathbf{V}}^T\mathbf{G}^{-1}\dot{\tilde{\mathbf{V}}}\right\}.\end{aligned} \tag{4.111}$$

After applying the update laws designed in (4.98), canceling out the matched terms, and utilizing the definitions of (4.102), (4.111) can be upperbounded as follows

$$\dot{V}_2 \leq -\mathbf{r}^T\mathbf{K}_v\mathbf{r} + \kappa\|\mathbf{r}\| tr\left\{\tilde{\mathbf{Z}}^T\left(\mathbf{Z} - \tilde{\mathbf{Z}}\right)\right\} + \|\mathbf{r}\|\|\mathbf{w}\| + \mathbf{r}^T\mathbf{v}. \tag{4.112}$$

By substituting (4.101) and (4.103) into (4.112), it is possible to further upperbound $\dot{V}_2$ as

$$\begin{aligned}\dot{V}_2 \leq \ & -\|\mathbf{r}\|\left[\mathbf{K}_{v_{\min}}\|\mathbf{r}\| - \kappa\left\|\tilde{\mathbf{Z}}\right\|_F\left(Z_B - \left\|\tilde{\mathbf{Z}}\right\|_F\right) - C_0 - C_1\left\|\tilde{\mathbf{Z}}\right\|_F\right. \\ & \left. -C_2\left\|\tilde{\mathbf{Z}}\right\|_F\|\mathbf{r}\| + K_z\left(\left\|\hat{\mathbf{Z}}\right\|_F + Z_B\right)\|\mathbf{r}\|\right]\end{aligned} \tag{4.113}$$

where the following relation has been used to derive (4.113)

$$\begin{aligned}tr\left\{\tilde{\mathbf{Z}}^T\left(\mathbf{Z} - \tilde{\mathbf{Z}}\right)\right\} \ &= \left\langle\tilde{\mathbf{Z}},\ \mathbf{Z}\right\rangle - \left\|\tilde{\mathbf{Z}}\right\|_F^2 \leq \left\|\tilde{\mathbf{Z}}\right\|_F\|\mathbf{Z}\|_F - \left\|\tilde{\mathbf{Z}}\right\|_F^2 \\ &\leq \left\|\tilde{\mathbf{Z}}\right\|_F Z_B - \left\|\tilde{\mathbf{Z}}\right\|_F^2.\end{aligned} \tag{4.114}$$

Based on the fact that $\left\|\hat{\mathbf{Z}}\right\|_F + Z_B > \left\|\tilde{\mathbf{Z}}\right\|_F$, one can choose $K_z > C_2$ such that (4.113) can be rewritten as

$$\dot{V}_2 \leq -\|\mathbf{r}\|\left[\mathbf{K}_{v_{\min}}\|\mathbf{r}\| - \kappa\left\|\tilde{\mathbf{Z}}\right\|_F\left(Z_B - \left\|\tilde{\mathbf{Z}}\right\|_F\right) - C_0 - C_1\left\|\tilde{\mathbf{Z}}\right\|_F\right]. \tag{4.115}$$

By defining $C_3 = Z_B + C_1/\kappa$, (4.115) can be rewritten as follows

$$\dot{V}_2 \leq -\|\mathbf{r}\| \left[K_{v_{\min}} \|\mathbf{r}\| + \kappa \left(\left\| \tilde{\mathbf{Z}} \right\|_F - C_3/2 \right)^2 - C_0 - \kappa C_3^2/4 \right] \tag{4.116}$$

where $K_{v_{\min}}$ denotes the minimum singular value of $\mathbf{K}_v$. Combining with (4.110), (4.116) can be upperbounded as follows

$$\dot{V}_0 \leq -\gamma \left(\|\mathbf{z}\|^2 \right) - \|\mathbf{r}\| \left[K_{v_{\min}} \|\mathbf{r}\| + \kappa \left(\left\| \tilde{\mathbf{Z}} \right\|_F - C_3/2 \right)^2 - C_0 - \kappa C_3^2/4 \right]. \tag{4.117}$$

It is straightforward to see that (4.117) is guaranteed negative as long as either

$$\|\mathbf{r}\| > \frac{C_0 + \kappa C_3^2/4}{K_{v_{\min}}} \equiv b_r \text{ or } \left\| \tilde{\mathbf{Z}} \right\|_F > C_3/2 + \sqrt{C_0 + \kappa C_3^2/4} \equiv b_Z \tag{4.118}$$

Thus, $\dot{V}_0$ is negative outside the compact set $\left\{ \|\mathbf{r}\| \leq b_r, \ \left\| \tilde{\mathbf{Z}} \right\|_F \leq b_Z \right\}$. Now, LaSalle extension in [46] can be used to prove the UUB results for both $\|\mathbf{r}\|$ and $\left\| \tilde{\mathbf{Z}} \right\|_F$. It is easy to see from (4.118) that the size of the ultimate bound b_r for $\|\mathbf{r}\|$ can be made smaller by increasing the size of the control gain. We note here that the gain matrix $\mathbf{K}$ needs to be chosen *appropriately large* in the sense that the selections for k_d and k_{Λ_1} are made to ensure that the parenthesized term in (4.109) is positive. ■

We assume that the only measurements available are the pitching and plunging displacements; thus, the remaining states are estimated through the use of a high gain observer (HGO). When $\mathbf{x}(t)$ is the output of the system and the only measurable state vector, the sole measurable error signal is $\mathbf{e}_1(t)$, given the knowledge of $\mathbf{x}(t)$ and $\mathbf{x}_d(t)$. Motivated by the result in [37], an estimate $\hat{\mathbf{z}}(t) = \left[\hat{\mathbf{e}}_1^T, \ \hat{\mathbf{e}}_2^T, \ \hat{\mathbf{r}}^T \right]^T \in \Re^6$ for the auxiliary error signal $\mathbf{z}(t)$ can be obtained via the following HGO

$$\dot{\hat{\mathbf{e}}}_1 = \hat{\mathbf{r}} - \mathbf{2}\hat{\mathbf{e}}_1 + \frac{\alpha_1}{\bar{\epsilon}} (\mathbf{e}_1 - \hat{\mathbf{e}}_1) \text{ and } \dot{\hat{\mathbf{r}}} = \frac{\alpha_2}{\bar{\epsilon}^2} (\mathbf{e}_1 - \hat{\mathbf{e}}_1) \tag{4.119}$$

where $\alpha_i \in \Re^{m\times m}\ \forall\ i = 1, 2$ are gain constants and $\bar{\epsilon}$ is a small positive constant. Note that $\hat{\mathbf{e}}_2 = \hat{\mathbf{r}} - \hat{\mathbf{e}}_1$. In order to suppress the peaking phenomenon due to using HGO, we modify the full-state control design of (4.87) to an output feedback saturated control as follows

$$\mathbf{u} = sat\left[\mathbf{D}^{-1}\left(\mathbf{K}\hat{\mathbf{r}} + \hat{\mathbf{N}} - \mathbf{v}\right)\right] \tag{4.120}$$

where $sat\,(\cdot)$ denotes the standard saturation function and saturation is applied outside an appropriately defined compact set for the control input $\mathbf{u}$. Here, $\hat{\mathbf{N}}$ and $\mathbf{v}$ have been defined in the same manner as in (4.87). For details of the stability analysis of the output feedback control design, the reader is referred to [37].

Simulation results were presented for a nonlinear 2-DOF aeroelastic system controlled by leading- and trailing- edge flaps and subjected to external disturbances. The nonlinear wing section model was simulated using the dynamics of (4.75) and (4.76). The model parameters utilized in the simulation were the same as used in [47] and listed in Table 4.1. In particular, the pitching spring stiffness $k_\alpha\,(\alpha)$ was modeled as a polynomial nonlinearity as shown in Table I. Note that all these parameters were used to simulate the wing model but were considered unknown for the purpose of control design.

Similar to [44] and [47], the desired trajectory variables $\mathbf{x}_d$, $\dot{\mathbf{x}}_d$, and $\ddot{\mathbf{x}}_d$ were simply selected as zero. The initial conditions for pitch angle $\alpha(t)$ and plunge displacement $h(t)$ were chosen as $\alpha(0) = 5.729$ [deg] and $h(0) = 0$ [m] while all other variables $\dot{h}(t)$, $\dot{\alpha}(t)$, $\ddot{h}(t)$, and $\ddot{\alpha}(t)$ were initially set to zero. Both the leading edge $\beta(t)$ and trailing edge $\gamma(t)$ flaps were constrained to vary between ± 15 [deg]. For the numerical example, the signs of the

Table 4.1: Wing Section Parameters

Parameter	Value	Parameter	Value
a	$= -0.6719$	b	$= 0.1905\ [\,\mathrm{m}\,]$
s	$= 0.5945\ [\,\mathrm{m}\,]$	ρ	$= 1.225\ [\,\mathrm{kg \cdot m^3}\,]$
r_{cg}	$= -b(.0998 + a)\ [\,\mathrm{m}\,]$	x_a	$= r_{cg}/b$
c_h	$= 27.43\ [\,\mathrm{kg\,/s}]$	c_α	$= 0.0360\ [\,\mathrm{N \cdot s}\,]$
k_h	$= 2844\ [\,\mathrm{N\,/\,m}\,]$	m_{wing}	$= 4.340\ [\,\mathrm{kg}\,]$
m_w	$= 5.23\ [\,\mathrm{kg}\,]$	m_T	$= 15.57\ [\,\mathrm{kg}\,]$
I_{cgw}	$= 0.04342\ [\,\mathrm{kg \cdot m^2}\,]$	I_{cam}	$= 0.04697\ [\,\mathrm{kg \cdot m^2}\,]$
$C_{l\alpha}$	$= 6.757\ [\,\mathrm{rad^{-1}}\,]$	$C_{m\alpha}$	$= 0\ [\,\mathrm{rad^{-1}}\,]$
$C_{l\beta}$	$= 3.774\ [\,\mathrm{rad^{-1}}\,]$	$C_{m\beta}$	$= -0.6719\ [\,\mathrm{rad^{-1}}\,]$
$C_{l\gamma}$	$= -0.1566\ [\,\mathrm{rad^{-1}}\,]$	$C_{m\gamma}$	$= -0.1005\ [\,\mathrm{rad^{-1}}\,]$
$k_\alpha\,(\alpha)$	$= 12.77 + 53.47\alpha + 1003\alpha^2\ [\mathrm{N \cdot m}]$		
I_α	$= I_{cam} + I_{cgw} + m_{wing} r_{cg}^2\ [\,\mathrm{kg \cdot m^2}\,]$		

leading principal minors of the high-frequency gain matrix $\mathbf{G}_s$ are encoded in the diagonal matrix $\mathbf{D}$ which can be explicitly given as

$$\mathbf{D} = \begin{bmatrix} -1 & 0 \\ 0 & -1 \end{bmatrix}. \tag{4.121}$$

We remark that the model-free controller designed here depends only on the knowledge of $\mathbf{D}$ but not on the knowledge of $\mathbf{S}$ and $\mathbf{U}$.

Before introducing the external disturbance tested, a simple static exploration of the wing section model reveals the relation between magnitude of sustained external disturbance and the amplitude-limited control signals. First, we assume that wing section model is able to reach the desired equilibrium point (*e.g.,* h, α, $\dot{h}$, $\dot{\alpha}$, $\ddot{h}$, and $\ddot{\alpha}$ are all equal to zero) under certain types of external disturbances. In this case, the left hand side of (4.75) is zero, and all terms associated with h, α, $\dot{h}$, and $\dot{\alpha}$ on the right hand side of (4.75) are also zero. Thus, it is straightforward to see that

$$\begin{cases} \rho U_\infty^2 bsC_{l\beta}\beta + \rho U_\infty^2 bsC_{l\gamma}\gamma + \rho U_\infty bsC_{l\alpha} w_G(\tau) &= 0, \\ \rho U_\infty^2 b^2 sC_{m\beta-eff}\beta + \rho U_\infty^2 b^2 sC_{m\gamma-eff}\gamma + \left(\frac{1}{2} - a\right) bL_g &= 0. \end{cases} \tag{4.122}$$

Based on the gust model, (4.122) can be simplified as

$$\begin{bmatrix} C_{l\beta} & C_{l\gamma} \\ C_{m\beta-eff} & C_{m\gamma-eff} \end{bmatrix} \begin{bmatrix} \beta \\ \gamma \end{bmatrix} = \begin{bmatrix} -C_{l\alpha} w_G(\tau)/U_\infty \\ -\left(\frac{1}{2} - a\right) C_{l\alpha} w_G(\tau)/U_\infty \end{bmatrix}. \tag{4.123}$$

Assuming the 2×2 matrix in above equation is non-singular, we have

$$\begin{bmatrix} \beta \\ \gamma \end{bmatrix} = -\frac{w_G(\tau)}{U_\infty} \begin{bmatrix} C_{l\beta} & C_{l\gamma} \\ C_{m\beta-eff} & C_{m\gamma-eff} \end{bmatrix}^{-1} \begin{bmatrix} C_{l\alpha} \\ \left(\frac{1}{2} - a\right) C_{l\alpha} \end{bmatrix}. \tag{4.124}$$

Now, it's easy to see that given bounded control signals β and γ, one can obtain an upper bound for the magnitude of $w_G(\tau)$ depending on the flow speed U_∞. If $w_G(\tau)$ is too large with respect to the constrained control signals, (4.122) will not hold and the wing section model variables α and h are unable to reach the origin regardless of the type of control design. Given the parameters listed in Table I, the maximum magnitude of the external signals cannot be larger than 0.047 [m / s] and 0.077 [m / s], corresponding to 0.58% of the velocities selected, for the two values of velocities selected in simulations, $U_\infty = 8$ [m / s] and $U_\infty = 13.28$ [m / s], respectively, in order to drive the plunge and pitch displacement to zero. As will be seen in the results, larger disturbance size results in alternate equilibria away from the origin.

In this simulation, three kinds of external disturbances are considered according to [43]. The first type of external disturbance is modeled as a triangular gust, whose velocity distribution $w_G(\tau)$ can be given as

$$w_G(\tau) = 2w_0\frac{\tau}{\tau_G}\left(H(\tau) - H\left(\tau - \frac{\tau_G}{2}\right)\right) - 2w_0\left(\frac{\tau}{\tau_G} - 1\right)\left(H(\tau - \tau_G) - H\left(\tau - \frac{\tau_G}{2}\right)\right) \tag{4.125}$$

where $H(\cdot)$ denotes a unit step function, $\tau_G = U_\infty t_G/b$ and $t_G = 0.25$ [s], and $w_0 = 0.7$ [m / s]. This triangular gust lasts 0.5 seconds from $t = 0$ [s] to $t = 0.5$ [s]. The second type of external disturbance – one that is sustained beyond the transient response time of the closed-loop aeroelastic system – is given in the form of graded gust, whose velocity distribution $w_G(\tau)$ can be expressed as follows

$$w_G(\tau) = H(\tau)\, w_0\left(1 - e^{-0.75\tau}\right) \tag{4.126}$$

where w_0 is chosen according to the simulation setting. The third disturbance is given in the form of sinusoidal gust with the following velocity distribution function $w_G(\tau)$

$$w_G(\tau) = H(\tau)\, w_0 \sin \omega\tau \tag{4.127}$$

where $\omega = 0.5$ [rad / s] while w_0 is selected based on different simulation settings. Thus, these three disturbances profiles test the system response to ephemeral disturbance, steady sustained disturbance, and time-varying sustained disturbance. Also note that the triangular gust tested is very similar to the traditional 1-cosine gust-type function - both of which can be classified as ephemeral disturbances. Furthermore, a more challenging continuous sinusoidal disturbance is also tested in the following simulation.

Both the leading edge $\beta(t)$ and trailing edge $\gamma(t)$ flaps are constrained to vary between ± 15 [deg], assuming that saturation will occur outside these limits. Since the control design contains a learning component that involves integration of the error system (see (4.98) where $\hat{\mathbf{W}}$ and $\hat{\mathbf{V}}$ rely upon integration of the filtered error signal $\hat{\mathbf{r}}$), control input saturation is known to lead to windup problem. Motivated by back-calculation algorithm introduced in [48], we propose the following method to limit the error signal $\hat{\mathbf{r}}$ according to the magnitude of original control input $\mathbf{u}_i$ in (4.98) as

$$r_{b,i} = \begin{cases} g_i \hat{r}_i \dfrac{u_b}{|u_i|} & , \ |u_i| > u_b, \ \forall i = 1, 2 \\ \hat{r}_i & , \ |u_i| \leq u_b, \ \forall i = 1, 2 \end{cases} \tag{4.128}$$

where $\mathbf{r}_b$ denotes the limited filtered error which is used in the neural network weight matrices update law, $\mathbf{u}$ designed in (4.120) denotes the actual control signal for the actuator with

saturation bound $u_b = 15$ [deg], while g_i, $i = 1, 2$ denote a set of auxiliary saturation gains. After limiting the error signal $\hat{\mathbf{r}}$ according to (4.128), the weight matrices update law for the neural networks compensator and robustifying term are modified as follows

$$\begin{aligned}
\dot{\hat{\mathbf{W}}} &= \left(\mathbf{F}\hat{\boldsymbol{\sigma}} - \mathbf{F}\hat{\boldsymbol{\sigma}}'\hat{\mathbf{V}}^T\bar{\mathbf{x}}\right)\mathbf{r}_b^T - \kappa\mathbf{F}\left\|\mathbf{r}_b\right\|\hat{\mathbf{W}}, \\
\dot{\hat{\mathbf{V}}} &= \mathbf{G}\mathbf{x}\left(\hat{\boldsymbol{\sigma}}'^T\hat{\mathbf{W}}\mathbf{r}_b^T\right)^T - \kappa\mathbf{G}\left\|\mathbf{r}_b\right\|\hat{\mathbf{V}}, \\
\mathbf{v} &= -K_z\left(\left\|\hat{\mathbf{Z}}\right\|_F + Z_B\right)\mathbf{r}_b.
\end{aligned} \tag{4.129}$$

The output feedback control is implemented via the high gain observer defined in (4.34) and control law in (4.120). The parameters for the controller and observer in these simulations are listed in Table 4.2.

Also note that an explicit expression for $\mathbf{D}$ has been given in (4.121). According to the definition of $\bar{\mathbf{x}}_t$ given in (4.93), a choice of $p_1 = 11$ needs to be made in general. For the numerical example, however, since $\mathbf{x}_d$, $\dot{\mathbf{x}}_d$, and $\ddot{\mathbf{x}}_d$ were all bounded signals and chosen to be zero for all time, they can be removed from the input set $\bar{\mathbf{x}}_t$ in order to simplify the computational complexity. The simplified input set for the numerical example is $\bar{\mathbf{x}}_t = \left[\mathbf{x}^T,\ \dot{\mathbf{x}}^T,\ \left\|\hat{\mathbf{Z}}\right\|_F\right]^T \in \Re^{\mathbf{5}}$ based upon which $\bar{\mathbf{x}} = [1,\ \bar{\mathbf{x}}_t]^T \in \Re^{\mathbf{6}}$. Then, in the feedforward compensator used in the following simulation, p_1, p_2, and p_3 are given as $p_1 = 5$, $p_2 = 10$, $p_3 = 2$. The above selection of p_1, p_2, and p_3 implies that $\hat{\mathbf{W}} \in \Re^{11\times 2}$ and $\hat{\mathbf{V}} \in \Re^{6\times 10}$. The number of hidden layer nodes is chosen through a trial and error method in order to obtain best performance. A choice of $p_2 = 10$ is used since the controller performance is seen to be satisfactory for this choice. Although the approximation error is expected to reduce when the number of hidden layer nodes increases, one still needs to consider the computational

Table 4.2: Control Gains

Parameter	Triangular		Graded	Sinusoidal
U_∞	8 [m / s]	13.28 [m / s]	13.28 [m / s]	13.28 [m / s]
$\mathbf{K}$	$3\mathbf{I}_{2\times2}$	$0.5\mathbf{I}_{2\times2}$	$0.5\mathbf{I}_{2\times2}$	$0.5\mathbf{I}_{2\times2}$
$\mathbf{F}$	$10\mathbf{I}_{11\times11}$	$5\mathbf{I}_{11\times11}$	$5\mathbf{I}_{11\times11}$	$5\mathbf{I}_{11\times11}$
$\mathbf{G}$	$200\mathbf{I}_{6\times6}$	$50\mathbf{I}_{6\times6}$	$50\mathbf{I}_{6\times6}$	$50\mathbf{I}_{6\times6}$
κ	0.4	0.6	0.6	0.01
K_z	0.1	0.1	0.1	10
Z_B	0.1	0.1	0.1	10
g_1	0.5	1	1	1
g_2	1	0.2	0.2	0.2
α_1	1	1	1	1
α_2	0.5	0.5	0.5	0.5
$\bar{\epsilon}$	0.001	0.005	0.005	0.0002

efficiency, especially considering the constraints of real-time control implementation. It is well known that arbitrary choices for the initial weight matrices $\hat{\mathbf{W}}$ and $\hat{\mathbf{V}}$ may result in unacceptable transient response. By performing extensive simulations, the initial weight matrix $\hat{\mathbf{W}}$ is chosen to be zero while the initial weights for elements of $\hat{\mathbf{V}}$ are randomly chosen between -1 and 1. Simulation results show that such a selection guarantees an acceptable transient response. The weight update laws for the neural networks compensator and the robustifying term have been defined in (4.129) after applying the anti-windup mechanism.

Three sets of simulations were run based on three types of external disturbances described above in (4.125), (4.126), and (4.127). The triangular gust disturbance defined in (4.125) was the first type of external disturbance considered in the simulation. Fig. 4.10(a) and Fig. 4.10(b) compare the closed-loop response of the system under the triangular gust between the control given in [44] and the proposed controller under a slightly stronger disturbance, namely, $w_0 = 0.7$ [m / s]. As one can see from Fig. 4.10(a), both plunge and pitch displacements keep oscillating and show no sign of convergence by using the method in [44]. However, Fig 4.10(b) shows that the proposed control drives the plunge and pitch displacement to zero in less than 3 [s]. The oscillatory behavior seen in Fig. 4.10(a) stems from the lack of an anti-windup mechanism in [44]. In this set of simulations, we first choose a small graded gust $w_0 = 0.07$ [m / s] such that both plunge and pitch displacements are able to converge to zero within the actuator limitations. From Fig. 4.11, one can easily observe the convergence of the error to the origin under the adaptive method of [44] and the proposed method. Also in this case, the proposed method shows faster settling times. Under a sinusoid-like gust with

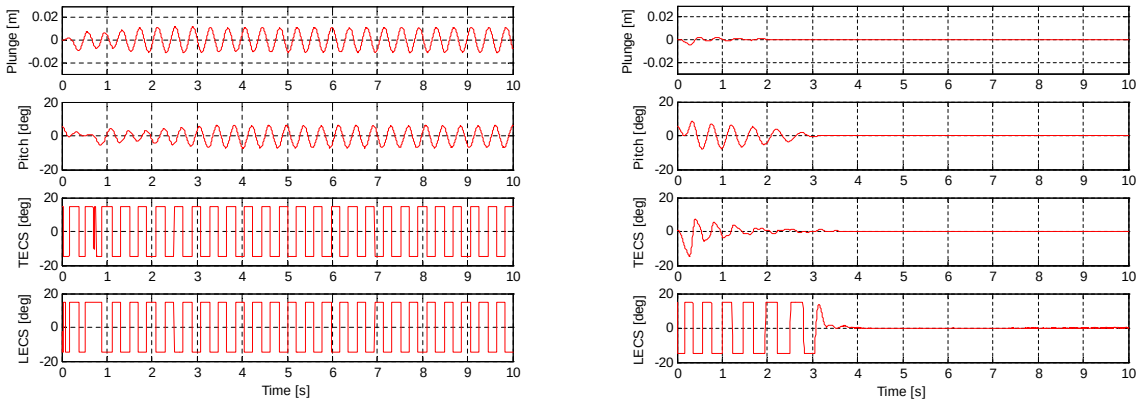

(a) (b)

Figure 4.10: Closed loop response under triangular gust $w_0 = 0.7[m/s]$ at pre-flutter speed $U_\infty = 8[m/s]$ (a): using the method in [39]; (b): using the proposed method.

$w_0 = 0.07$ [m / s] at post flutter speed $U_\infty = 13.28$ [m / s]$> U_F = 11.4$ [m / s], Fig. 4.12(a) shows that the method in [44] needs more than 5 [s] to stabilize the system. However, the proposed method successfully stabilizes the system in less than 1.5 [s].

Here we note that since the simulation results under the triangular gust and a more challenging continuous sinusoidal gust are satisfactory, one can expect satisfactory simulation results under other similar disturbances, such as the 1-cosine gust-type disturbance. Generally speaking, the proposed model free output feedback controller designed shows substantially greater robustness with respect to modeling uncertainty and various external disturbances as compared with the adaptive backstepping results obtained in [44].

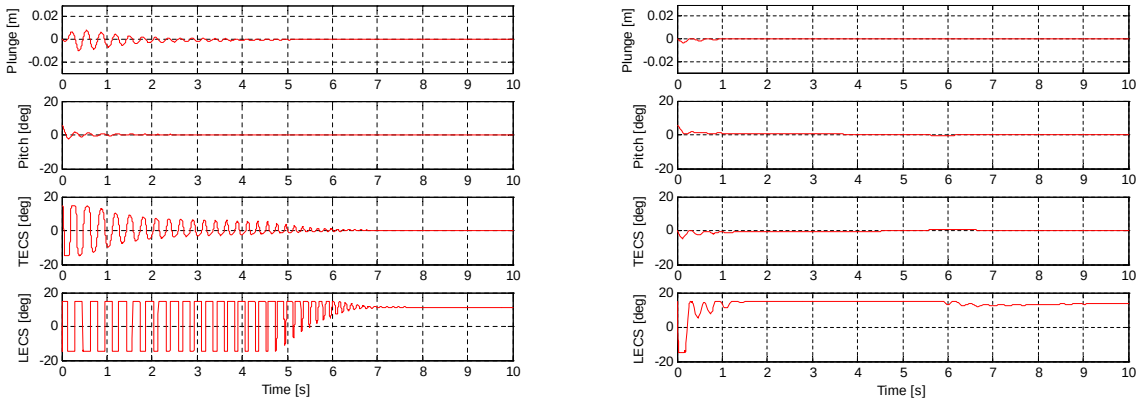

(a) (b)

Figure 4.11: Closed loop response under graded gust $w_0 = 0.07[m/s]$ at post-flutter speed $U_\infty = 13.28[m/s]$ (a): using the method in [39]; (b): using the proposed method.

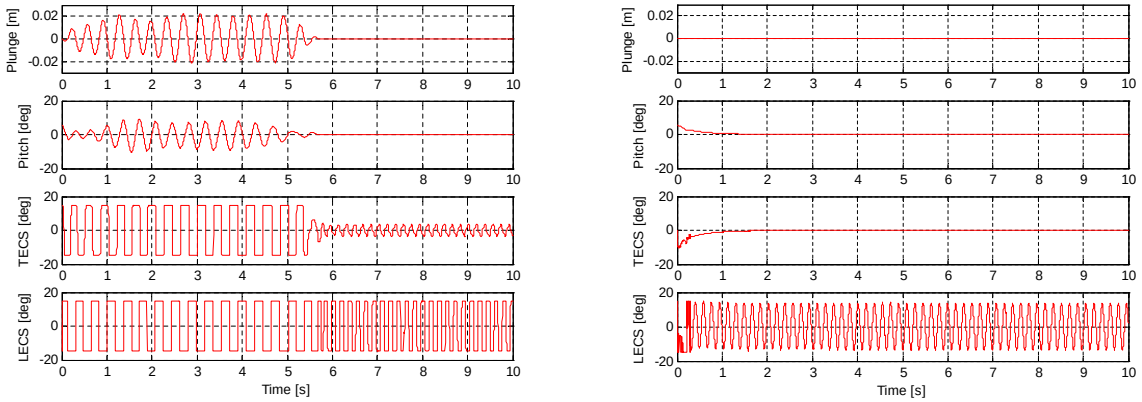

(a) (b)

Figure 4.12: Closed loop response under sinusoidal gust $w_0 = 0.07[m/s]$ at post-flutter speed $U_\infty = 13.28[m/s]$ (a): using the method in [39]; (b): using the proposed method.

4.4 Continuous Robust Control Design for 2-DOF MIMO Nonlinear System

Here, the following subclass of MIMO nonlinear systems with two DOFs is considered

$$x^{(n)} = h\left(\mathbf{x}, x^{(n-1)}\right) + G\left(\mathbf{x},\theta\right) u \tag{4.130}$$

where $x^{(i)}\left(t\right) \in \mathbb{R}^2$, $i = 0, 1, ..., n-1$ denote the system states while $\mathbf{x} \triangleq \left[\begin{array}{cccc} x^T & \dot{x}^T & \ldots & \left(x^{(n-2)}\right)^T \end{array}\right]^T \in \mathbb{R}^{2n-4}$, $x(t) \in \mathbb{R}^2$ is the system output and $u\left(t\right) \in \mathbb{R}^2$ is defined to be the control input. The drift vector $h\left(\mathbf{x},x^{(n-1)}\right) \in \mathbb{R}^2$ is assumed to be a $\mathcal{C}^2$ nonlinear function with unstructured uncertainty. The high frequency gain matrix $G\left(\mathbf{x},\theta\right) \in \mathbb{R}^{2\times 2}$ is also a $\mathcal{C}^2$ nonlinear function and affine in the unknown constant parameter vector $\theta \in \mathbb{R}^p$. For the purpose of robust control design, we assume that $G\left(\mathbf{x},\theta\right)$ is a real matrix with nonzero leading principal minors whose signs are assumed to be known. In order to facilitate the continuous robust control design, we begin by differentiating (4.130) which yields the following expression

$$x^{(n+1)} = f\left(\mathbf{x},x^{(n-1)}, x^{(n)}\right) + G\left(\mathbf{x},\theta\right) \dot{u} \tag{4.131}$$

where $f\left(\mathbf{x},x^{(n-1)}, x^{(n)}\right)$ is defined as

$$f\left(\cdot\right) = \dot{h}\left(\mathbf{x},x^{(n-1)}\right) + \dot{G}\left(\mathbf{x},\theta\right) G^{-1}\left(\mathbf{x},\theta\right)\left(x^{(n)} - h\left(\mathbf{x},x^{(n-1)}\right)\right). \tag{4.132}$$

By applying the matrix decomposition approach introduced in Lemma 1, HFG matrix $G\left(\mathbf{x},\theta\right)$ can be factorized as $G\left(\mathbf{x},\theta\right) = S\left(\mathbf{x},\theta\right) U\left(\mathbf{x},\theta\right)$ given the assumption that $G\left(\mathbf{x},\theta\right)$ is a real matrix with nonzero leading principal minors. After taking SDU decomposition result into (4.131) and premultiplying $M\left(\mathbf{x},\theta\right)$ on both sides of the equation, one can get

the following result

$$M\left(\mathbf{x},\theta\right)x^{(n+1)} = \varphi\left(\mathbf{x},x^{(n-1)},x^{(n)},\theta\right) + DU\left(\mathbf{x},\theta\right)\dot{u} \tag{4.133}$$

where S, U, and D have been previously defined, $M\left(\mathbf{x},\theta\right) \triangleq S^{-1}\left(\mathbf{x},\theta\right) \in \mathbb{R}^{2\times 2}$ is a symmetric and positive definite matrix while $\varphi\left(\mathbf{x},x^{(n-1)},x^{(n)},\theta\right) \triangleq M\left(\mathbf{x},\theta\right) \cdot f\left(\mathbf{x},x^{(n-1)},x^{(n)}\right) \in \mathbb{R}^2$ is an unknown auxiliary vector with unstructured uncertainty.

The tracking error $e_1 \in \mathbb{R}^2$ can be defined as (4.6). Furthermore, the following auxiliary error signals $e_i \in \mathbb{R}^2 \; \forall \; i = 2, ...n$ are utilized

$$\begin{aligned} e_2 &= \dot{e}_1 + e_1, \\ e_3 &= \dot{e}_2 + e_2 + e_1, \\ &\vdots \\ e_n &= \dot{e}_{n-1} + e_{n-1} + e_{n-2}. \end{aligned} \tag{4.134}$$

The result in [34] shows that e_i can be expressed as

$$e_i\left(t\right) = \sum_{j=0}^{i-1} c_{ij} e_1^{(j)}\left(t\right) \qquad \forall \; i = 2, 3, ..., n \tag{4.135}$$

where the known constant coefficients c_{ij} are generated via a Fibonacci number series [34]. Based on above definitions, the filtered error signal $r\left(t\right) \in \mathbb{R}^2$ and $z\left(t\right) \in \mathbb{R}^{2n+2}$ can be defined as follows

$$r = \dot{e}_n + \alpha e_n, \quad z \triangleq \begin{bmatrix} e_1^T & e_2^T & ... & e_n^T & r^T \end{bmatrix}^T \tag{4.136}$$

where α is a positive gain constant. After taking the time derivative of r in (4.136) and utilizing (4.133), (4.6), (4.134), and (4.135), one can obtain the open-loop dynamics as

follows

$$\begin{aligned} M\dot{r} = \; & M\left(x_d^{(n+1)} + \sum_{j=0}^{n-2} c_{ij} e_1^{(j+2)} + \alpha \dot{e}_n\right) \\ & -\varphi\left(\mathbf{x},x^{(n-1)},x^{(n)},\theta\right) + e_n + \Pi - D\dot{u} - e_n \end{aligned} \tag{4.137}$$

where $\bar{U}(\mathbf{x},\theta) \in \mathbb{R}^{2\times 2}$ is a strictly upper triangular matrix while $\Pi \in \mathbb{R}^2$ is an auxiliary vector with the following definitions

$$\begin{aligned} & \bar{U}(\mathbf{x},\theta) \triangleq D - DU(\mathbf{x},\theta), \\ & \Pi \triangleq \bar{U}(\mathbf{x},\theta)\,\dot{u} = \begin{bmatrix} \bar{U}_{12}(\mathbf{x},\theta)\,\dot{u}_2 & 0 \end{bmatrix}^T. \end{aligned} \tag{4.138}$$

In order to facilitate the full state control design for above open-loop dynamics, (4.139) can be rewritten in a compact form as

$$M\dot{r} = -\frac{1}{2}\dot{M}r + N + \Pi - D\dot{u} - e_n \tag{4.139}$$

where $N(\cdot) \in \mathbb{R}^2$ in (4.139) is defined as

$$\begin{aligned} N = \; & M\left(x_d^{(n+1)} + \sum_{j=0}^{n-2} c_{ij} e_1^{(j+2)} + \alpha \dot{e}_n\right) - \varphi\left(\mathbf{x},x^{(n-1)},x^{(n)},\theta\right) + e_n + \tfrac{1}{2}\dot{M}r \\ = \; & N_d + \tilde{N}_0 \end{aligned} \tag{4.140}$$

where $N_d = N\left(\mathbf{x}_d, x_d^{(n)}, x_d^{(n+1)}\right) \in \mathbb{R}^2$ and $\tilde{N}_0 = N - N_d \in \mathbb{R}^2$. Then, it can be easily verified that $\|N_d\|$, $\left\|\dot{N}_d\right\| \in \mathcal{L}_\infty$ given the smoothness of the desired trajectory as given by (3.2) and the fact that $\varphi\left(\mathbf{x},x^{(n-1)},x^{(n)},\theta\right)$ is a $\mathcal{C}^1$ function. Furthermore, by using the fact that N is continuously differentiable, $\left\|\tilde{N}_0\right\|$ can be upperbounded as

$$\left\|\tilde{N}_0\right\| \leq \rho_0(\|z\|)\,\|z\| \tag{4.141}$$

where $\rho_0(\cdot)$ is a global invertible nondecreasing function and will be used in the ensuing stability analysis.

By assuming that all the state variables $\mathbf{x}$ are measurable, we can design a continuous robust feedback control law as follows

$$\begin{aligned} u(t) = \; & D^{-1}\left\{(K+I_2)\, e_n(t) - (K+I_2)\, e_n(0)\right. \\ & \left. + \int_0^t \left[\hat{\Phi} + (K+I_2)\,\alpha e_n(\tau) + \Gamma \text{sign}\left(e_n(\tau)\right)\right] d\tau \right\} \end{aligned} \tag{4.142}$$

where $K = K_p + diag\{K_{d,1}, 0\} \in \mathbb{R}^{2\times 2}$ and $\Gamma \in \mathbb{R}^{2\times 2}$ are both diagonal gain matrices, $I_2 \in \mathbb{R}^{2\times 2}$ is an identity matrix, $\hat{\Phi}(t) \triangleq \begin{bmatrix} Y\hat{\theta} & 0 \end{bmatrix}^T \in \mathbb{R}^2$, while $Y(\cdot)$ and $\hat{\theta}(t)$ will be defined later. In view of (4.142), the time derivative of $u(t)$ yields

$$\begin{aligned} \dot{u}_1 = \; & D_{1,1}^{-1}\left[Y\hat{\theta} + (K_{1,1}+1)\, r_1 + \Gamma_{1,1}\text{sign}\left(e_{n,1}\right)\right], \\ \dot{u}_2 = \; & D_{2,2}^{-1}\left[(K_{2,2}+1)\, r_2 + \Gamma_{2,2}\text{sign}\left(e_{n,2}\right)\right] \end{aligned} \tag{4.143}$$

where $\dot{u}_i(t)$ denotes the i^{th} element in $\dot{u}(t)$, $D_{i,i}$, $K_{i,i}$, and $\Gamma_{i,i}$ denote the i^{th} diagonal element in the matrices D, K, and Γ, respectively, while $e_{n,i}(t)$ and $r_i(t)$ represent the i^{th} element in auxiliary error signal $e_n(t)$ and filtered error signal $r(t)$, respectively. Note that $u_2(t)$ is readily implementable since $e_{n,2}(t)$ is measurable. $Y\hat{\theta}$ in $u_1(t)$ is designed to tackle the coupling-related disturbance terms $\bar{U}_{12}(\mathbf{x},\theta)\,\dot{u}_2$, which we write explicitly as follows

$$\begin{aligned} \Pi \; &= \begin{bmatrix} \bar{U}_{12}(\mathbf{x},\theta)\, D_{2,2}^{-1}\left[(K_{2,2}+1)\, r_2 + \Gamma_{2,2}\text{sign}\left(e_{n,2}\right)\right] \\ 0 \end{bmatrix} \\ &= \Lambda + \Phi \end{aligned} \tag{4.144}$$

where we have obtained the expression in (4.144) by substituting for $\dot{u}_2(t)$ from (4.143) into (4.138). Furthermore, $\Phi \in \mathbb{R}^2$ is a discontinuous auxiliary vector defined as follows

$$\Phi = \begin{bmatrix} Y\theta & 0 \end{bmatrix}^T \tag{4.145}$$

while $\Lambda \in \mathbb{R}^2$ is an auxiliary vector defined as follows

$$\Lambda = \begin{bmatrix} \Lambda_1 & 0 \end{bmatrix}^T \tag{4.146}$$

where $Y \triangleq D_{2,2}^{-1}\Gamma_{2,2}\text{sign}(e_{n,2})\, Y_{12} \in \mathbb{R}^{1\times p}$ is a regression vector, while θ is an unknown parameter vector and we have utilized the fact that $\bar{U}_{12}(\mathbf{x},\theta)$ can be parameterized as $\bar{U}_{12}(\mathbf{x},\theta) = Y_{12}(\mathbf{x})\,\theta$. We note here that the portion of the disturbance represented by (4.145) cannot be handled via a robustifying term because of its discontinuous nature; however, since Φ is affine in the uncertainty, it can be handled via adaptation as will be shown subsequently. Also note that $\Lambda_1 \triangleq \Delta(\mathbf{x})\, r_2 \in \mathbb{R}$ where $\Delta(\mathbf{x}) \triangleq D_{2,2}^{-1}\bar{U}_{1,2}(\mathbf{x},\theta)\,(K_{2,2}+1)$. After adding and subtracting the term $\Delta_d \triangleq \Delta(\mathbf{x}_d) \in \mathbb{R}$ to Δ, one can obtain

$$\Delta = \tilde{\Delta} + \Delta_d \tag{4.147}$$

where $\tilde{\Delta} = \Delta(\mathbf{x}) - \Delta_d(\mathbf{x}_d) \in \mathbb{R}$ and $\|\Delta_d\| \in \mathcal{L}_\infty$ based on the boundedness of $\mathbf{x}_d$. By using the fact that $U(\mathbf{x},\theta)$ is continuously differentiable, $\left\|\tilde{\Delta}\right\|$ can be further bounded as

$$\left\|\tilde{\Delta}\right\| \leq \rho_\Delta(\|z\|)\,\|z\| \tag{4.148}$$

where $\rho_\Delta(\cdot)$ is a global invertible nondecreasing function. Thus, $\Lambda_1 = \left[\tilde{\Delta} + \Delta_d(\mathbf{x}_d)\right] r_2$ can be upperbounded as

$$\begin{aligned} \|\Lambda_1\| &\leq \left\|\tilde{\Delta} + \Delta_d(\mathbf{x}_d)\right\| \|r_2\| \\ &\leq \left[\rho_\Delta(\|z\|)\,\|z\| + \|\Delta_d\|\right] \|z\| \\ &\leq \rho_1(\|z\|)\,\|z\| \end{aligned} \tag{4.149}$$

where $\rho_1(\cdot)$ is a global invertible nondecreasing function which depends on the gain $K_{2,2}$ – this fact would be utilized in the ensuing stability analysis. We note that the coupling-related

disturbance term $\bar{U}_{12}(\mathbf{x},\theta)\,\dot{u}_2$ has been separated into two parts Φ and Λ. While the latter term (which is continuously differentiable) will be compensated by nonlinear damping and the sign function based robustifying term, the former term (which is discontinuous) needs to be dealt with adaptively. Thus, one can define the parameter dynamic estimate as $\hat{\theta} \in \mathbb{R}^p$ and the corresponding mismatch as $\tilde{\theta} = \theta - \hat{\theta} \in \mathbb{R}^p$. Motivated by structure of Y and the following stability analysis, the adaptation law for $\hat{\theta}$ can be designed as follows

$$\begin{aligned} \hat{\theta}(t) = & \int_{t_0}^{t} \Gamma_Y Y r_1 d\tau \\ = & \int_{t_0}^{t} \Gamma_Y Y \dot{e}_{n,1} d\tau + \int_{t_0}^{t} \Gamma_Y Y \alpha e_{n,1} d\tau \end{aligned} \tag{4.150}$$

where $\Gamma_Y \triangleq \gamma_Y I$ and $I \in \mathbb{R}^{p\times p}$ is a identity matrix while γ_Y is a positive constant. It is important to note that r_1 is unmeasurable since it depends on $\dot{e}_{n,1}$ which in turn depends on $x^{(n)}$ which is not a state variable for the original system model given by (4.130) and is therefore considered unmeasurable. Therefore, the adaptation law cannot be implemented directly in the form shown in (4.150). Based on the known value of sign$(e_{n,2})$ and using additivity of integration on intervals, the integral term associated with unknown value $\dot{e}_{n,1}$ in (4.150) can be rewritten as

$$\int_{t_0}^{t} \Gamma_Y Y \dot{e}_{n,1} d\tau = k \sum_{j=1}^{n} \int_{t_{j,0}^{+}}^{t_{j,f}^{+}} Y_{12} \dot{e}_{n,1} d\tau - k \sum_{k=1}^{m} \int_{t_{k,0}^{-}}^{t_{k,f}^{-}} Y_{12} \dot{e}_{n,1} d\tau \tag{4.151}$$

where $k = \Gamma_Y D_{2,2}^{-1} \Gamma_{2,2}$ and

$$\text{sign}(e_{n,2}) = \begin{cases} 1, & \forall\, t \in \left(t_{j,0}^{+},\, t_{j,f}^{+}\right),\quad j = 1, ..., n \\ -1, & \forall\, t \in \left(t_{k,0}^{-},\, t_{k,f}^{-}\right),\ k = 1, ..., m \\ 0, & \text{otherwise.} \end{cases} \tag{4.152}$$

Also note that $(0,\, t] = T^+ \cup T^-$ where $T^+ = \bigcup_{j=1}^{n} \left(t_{j,0}^+,\, t_{j,f}^+\right]$ and $T^- = \bigcup_{k=1}^{m} \left(t_{k,0}^-,\, t_{k,f}^-\right]$. Then, integration by parts can be utilized in each interval in T^+ and T^- as

$$\begin{aligned} \hat{\theta}(t) = \quad & k\sum_{j=1}^{n}\left[Y_{12}e_{n,1}\big|_{t_{j,0}^+}^{t_{j,f}^+} - \int_{t_{j,0}^+}^{t_{j,f}^+} \dot{Y}_{12}e_{n,1}(\tau)\, d\tau\right] \\ & -k\sum_{k=1}^{m}\left[Y_{12}e_{n,1}\big|_{t_{k,0}^-}^{t_{k,f}^-} - \int_{t_{k,0}^-}^{t_{k,f}^-} \dot{Y}_{12}e_{n,1}(\tau)\, d\tau\right] + \int_0^t \Gamma_Y Y \alpha e_{n,1} d\tau. \end{aligned} \tag{4.153}$$

Since $e_{n,1}, Y_{12}(\mathbf{x}), \dot{Y}_{12}\left(\mathbf{x}, x^{(n-1)}\right)$ are measurable, thus $\hat{\theta}(t)$ is implementable in the form shown above. Finally, after substituting (4.143) into (4.139), one can obtain the following closed loop error dynamics

$$M\dot{r} = -\frac{1}{2}\dot{M}r + N_d + \tilde{N}_0 + \Lambda + \tilde{\Phi} - (K+I)\, r - \Gamma \mathrm{sign}(e_n) - e_n \tag{4.154}$$

where N_d and $\tilde{N}_0$ have been defined previously and $\tilde{\Phi} \triangleq \begin{bmatrix} Y\tilde{\theta} & 0 \end{bmatrix}^T$.

Before we proceed to analyze the stability of the closed-loop system under the control design proposed previously, we state the following two lemmas

Lemma 2 *For the following auxiliary function* $L(t) \in \mathbb{R}$

$$L = r^T\left(N_d - \Gamma\, sign(e_n)\right), \tag{4.155}$$

if the control gain matrix Γ *is chosen as*

$$\Gamma_{i,i} > \|N_{d,i}\|_{\mathcal{L}\infty} + \frac{1}{\alpha}\left\|\dot{N}_{d,i}\right\|_{\mathcal{L}\infty} \qquad \forall\ i = 1, 2 \tag{4.156}$$

where $N_{d,i}$ *is the* i^{th} *element in the vector* N_d*, then we can obtain*

$$\int_0^t L(\tau)\, d\tau \le \varsigma_L \tag{4.157}$$

where $\varsigma_L = \sum_{i=1}^{2} \Gamma_{i,i}\left|e_{n,i}(0)\right| - e_{n,i}(0)\, N_{d,i}(0)$.

Proof. The proof for this lemma can be adapted readily from [34]. ■

Lemma 3 *Consider a system* $\dot{\eta} = h(\eta, t)$ *where* $h : \mathbb{R}^m \times \mathbb{R}_{\geq 0} \to \mathbb{R}^m$ *and the solution exists. Defining the region* $D \subset \mathbb{R}^m$ *and* $D := \{\eta \in \mathbb{R}^m | \, \|\eta\| < \varepsilon\}$ *where* ε *is some positive constant, if there exists a continuously differentiable function* $V : D \times \mathbb{R}_{\geq 0} \to \mathbb{R}_{\geq 0}$ *such that*

$$W_1(\eta) \leq V(\eta, t) \leq W_2(\eta) \quad \text{and} \quad \dot{V}(\eta, t) \leq -W(\eta) \tag{4.158}$$

where $W_1(\cdot)$ *and* $W_2(\cdot)$ *are continuous positive-definite functions while* $W(\cdot)$ *is a uniformly continuous positive semidefinite function, and if* $\eta(0) \in S$ *where the region of attraction is defined as*

$$S := \left\{ \eta \in D | W_2(\eta) < \min_{\|\eta\| = \varepsilon} W_1(\eta) \right\},$$

then, it can be shown that

$$W(\eta) \to 0 \quad \text{as} \quad t \to \infty. \tag{4.159}$$

Proof. The proof for this lemma can be found in Theorem 8.4 of [37]. ■

Theorem 5 *Provided the control gain matrix* K *defined in (4.142) is chosen to be large enough,* $\alpha > 1/2$*, and* Γ *is selected according to (4.156), the proposed robust control design ensures that all the error signals* $e_1^{(i)} \to 0$ *as* $t \to \infty \quad \forall \; i = 1, ..., n$.

Proof. First, a non-negative Lyapunov function candidate V_0 is defined as

$$V_0(y, t) = \frac{1}{2} \sum_{i=1}^{n} e_i^T e_i + \frac{1}{2} r^T M r + \frac{1}{2} \tilde{\theta}^T \Gamma_Y^{-1} \tilde{\theta} + P \tag{4.160}$$

where the non-negative auxiliary function P can be defined as follows

$$P = \varsigma_L - \int_0^t L(\tau)\, d\tau \tag{4.161}$$

and $y = \begin{bmatrix} z & \tilde{\theta} & \sqrt{P} \end{bmatrix}^T \in \mathbb{R}^{2n+4}$. Based on the fact that $M(\mathbf{x},\theta)$ is positive definite, one can prove that $\underline{M} \leq M(\mathbf{x},\theta) \leq \bar{M}(\|y\|)$ where $\underline{M}$ is a positive constant and $\bar{M}(\cdot)$ is a nondecreasing function. Thus, V_0 in (4.160) can be bounded as follows

$$\lambda_1 \|y\|^2 \leq V_0(y,t) \leq \lambda_2(\|y\|)\|y\|^2$$

$$W_1(y) = \lambda_1 \|y\|^2 \quad \text{and} \quad W_2(y) = \lambda_2(\|y\|)\|y\|^2$$

where $\lambda_1 = \frac{1}{2}\min\left\{1,\ \underline{M},\ \Gamma_Y^{-1}\right\}$, and $\lambda_2 = \frac{1}{2}\max\left\{2,\ \bar{M}(\|y\|),\ \Gamma_Y^{-1}\right\}$. Upon taking the time derivative of (4.160) and utilizing (4.161), we obtain

$$\dot{V}_0 = \sum_{i=1}^{n} e_i^T \dot{e}_i + r^T M \dot{r} + \frac{1}{2} r^T \dot{M} r + \tilde{\theta}^T \Gamma_Y^{-1} \dot{\tilde{\theta}}^T - L. \tag{4.162}$$

By substituting from (4.6), (4.134), (4.136), (4.150), (4.154), (4.155), and utilizing the fact that $ab \leq \frac{1}{2}a^T a + \frac{1}{2}b^T b$, an upper bound for (4.162) can be obtained as

$$\begin{aligned} \dot{V}_0 \leq \ & -\sum_{i=1}^{n-2} e_i^T e_i - \tfrac{1}{2} e_{n-1}^T e_{n-1} - \left(\alpha - \tfrac{1}{2}\right) e_n^T e_n - \|r\|^2 \\ & + \|r\| \left\| \tilde{N}_0 \right\| + \|r\| \|\Lambda\| - \lambda_K \|r\|^2 - K_{d,1} r_1^2 \end{aligned} \tag{4.163}$$

where $\alpha > 1/2$ and λ_K is the maximum eigenvalue for the gain matrix K_p. Thus, $\dot{V}_0$ can be further upperbounded as

$$\dot{V}_0 \leq -\lambda_3 \|z\|^2 + \rho_0(\|z\|)\|r\|\|z\| - \lambda_K \|r\|^2 - K_{d,1} r_1^2 + r_1 \rho_1(\|z\|)\|z\| \tag{4.164}$$

where $\lambda_1 = \min\{1/2,\ (\alpha - 1/2)\}$. Then, by adding and subtracting term $\dfrac{\rho_0^2(\|z\|)}{4\lambda_K}\|z\|^2$ and $\dfrac{\rho_1^2(\|z\|)}{4K_{d,1}}\|z\|^2$ to the right hand side of the above inequality and utilizing a nonlinear damping

argument, one can further upperbound $\dot{V}_0$ as follows

$$\dot{V}_0 \leq -\lambda_4 \|z\|^2 - \left(\frac{\lambda_3 - \lambda_4}{2} - \frac{\rho_0^2(\|z\|)}{4\lambda_K}\right)\|z\|^2 - \left(\frac{\lambda_3 - \lambda_4}{2} - \frac{\rho_1^2(\|z\|)}{4K_{d,1}}\right)\|z\|^2. \quad (4.165)$$

Given a positive constant $\lambda_4 < \lambda_3$, one can first choose K_p such that $\lambda_K > \frac{\rho_0^2(||z||)}{2(\lambda_3 - \lambda_4)}$ or equivalently $z(t) \in \mathcal{D}_1$ where

$$\mathcal{D}_1 \triangleq \left\{ z \mid \|z\| < \rho_0^{-1}\left(\sqrt{2\lambda_K(\lambda_3 - \lambda_4)}\right)\right\}.$$

This ensures that the first parenthesized term in (4.165) is non-negative. Since $K \triangleq K_p + diag\{K_{d,1}, 0\}$, it is clear to see that $K_{2,2}$ is determined only by K_p and is independent of $K_{d,1}$. Then, based on the fact that ρ_1 depends on $K_{2,2}$, one can select $K_{d,1}$ large enough such that $K_{d,1} > \frac{\rho_1^2(\|z\|)}{2(\lambda_3 - \lambda_4)}$ or $z(t) \in \mathcal{D}_2$ where

$$\mathcal{D}_2 \triangleq \left\{ z \mid \|z\| < \rho_1^{-1}\left(\sqrt{2K_{d,1}(\lambda_3 - \lambda_4)}\right)\right\},$$

and $\mathcal{D}_1 \cap \mathcal{D}_2$ is non-empty. Motivated by Lemma 3 and the definition of y, $\mathcal{D}_1$, and $\mathcal{D}_2$, a region $\mathcal{D}$ can be defined as

$$\mathcal{D} \triangleq \left\{ y \mid \|y\| < \rho_0^{-1}\left(\sqrt{2\lambda_K(\lambda_3 - \lambda_4)}\right)\right\} \cap \left\{ y \mid \|y\| < \rho_1^{-1}\left(\sqrt{2K_{d,1}(\lambda_3 - \lambda_4)}\right)\right\}.$$

Thus, it is straightforward to prove that

$$\dot{V}_0 \leq -\lambda_4 \|z\|^2 = -W(y), \quad \forall\, y \in \mathcal{D}. \quad (4.166)$$

From (4.160) and (4.166), it is known that $V_0 \in \mathcal{L}_\infty$, and it is also straightforward to see that e_i, r, $\tilde{\theta}$, $\hat{\theta} \in \mathcal{L}_\infty$ $\forall\, i = 1, ..., n$. Then, by using (4.135), one can easily see that $e_1^{(i)} \in \mathcal{L}_\infty$ $\forall\, i = 1, ..., n-1$. Then, by using (4.134) and (4.136), one can easily see that $\dot{e}_i \in \mathcal{L}_\infty$

$\forall\ i = 1, ..., n$ which further implies that $e_1^{(n)} \in \mathcal{L}_\infty$ Next, given the fact that x_d is $\mathcal{C}^{n+2}$ smooth and $e_1^{(i)} \in \mathcal{L}_\infty\ \forall\ i = 1, ..., n$, it is possible to show that $x^{(i)} \in \mathcal{L}_\infty\ \forall\ i = 1, ..., n$ and $f\left(\mathbf{x}, x^{(n-1)}, x^{(n)}\right), G\left(\mathbf{x}, \theta\right) \in \mathcal{L}_\infty$ by using the definition in (4.6). Now, by utilizing (4.130), one can show that $u \in \mathcal{L}_\infty$. Based on the fact that $r \in \mathcal{L}_\infty$, we can see that $\dot{u}_2 \in \mathcal{L}_\infty$ according to (4.143). $Y \in \mathcal{L}_\infty$ based on the boundedness on x_d and e_i. Then, according to previous boundedness result on $\hat{\theta}$, one can also prove that $\dot{u}_1 \in \mathcal{L}_\infty$ given the definition in (4.143), which further implies $\dot{r} \in \mathcal{L}_\infty$ by using the definition in (4.139). Thus, given the facts that e_i, $\dot{e}_i$, r, $\dot{r} \in \mathcal{L}_\infty\ \forall\ i = 1, ..., n$, one can draw the conclusion that $\dot{W} = -\lambda_4 z^T \dot{z} \in \mathcal{L}_\infty$ which implies that $W\left(y\right)$ is uniformly continuous. Based on the definition of $\mathcal{D}$, one can also define a region S as

$$S \triangleq \left\{ y \in \mathcal{D}\ | W_2\left(y\right) < \lambda_1 \left(\rho_0^{-1}\left(\sqrt{2\lambda_K\left(\lambda_3 - \lambda_4\right)}\right)\right)^2 \right\} \cap \left\{ y \in \mathcal{D}\ | W_2\left(y\right) < \lambda_1 \left(\rho_1^{-1}\left(\sqrt{2K_{d,1}\left(\lambda_3 - \lambda_4\right)}\right)\right)^2 \right\}.$$

Now, one can use Lemma 3 to prove $\|z\| \to 0$ as $t \to \infty\ \forall\ y\left(0\right) \in S$. From (4.136), one can see that $e_i\left(t\right), r\left(t\right) \to 0$ as $t \to \infty\ \forall\ i = 1, ..., n$. By using (4.135), one can recursively prove that that $e_1^{(i)} \to 0\ \forall\ i = 1, ..., n$, as $t \to \infty$. Also note that region of attraction S in this problem can be made arbitrarily large to include any initial condition by choosing a large enough control gain. The above facts imply that our stability result is semi-global. ■

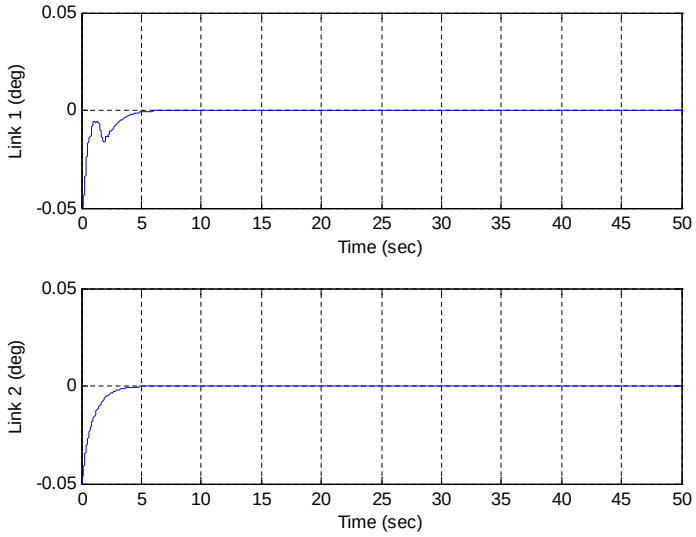

Figure 4.13: Robot link position tracking error under proposed robust control design.

4.4.1 Application to Robot Model

The proposed robust control design has been verified using numerical simulation through the same two DOF robot model defined in (4.37). The initial conditions of the robot manipulator have been set to $q_1(0) = q_2(0) = 0.05$ [rad] and $\dot{q}_1(0) = \dot{q}_2(0) = 0$ [rad $\cdot$ s^{-1}]. The parameter estimate is initialized as $\hat{\theta}(0) = 0$. The control gain K and Γ in (4.142), and the adaptation gain Γ_Y in (4.150) have been chosen as

$$K = diag\{5,\ 1\}, \quad \Gamma = 8I_2, \quad \Gamma_Y = 0.4.$$

The simulation result under full state feedback robust control law is demonstrated in Fig. 4.13. It is straightforward to see that the tracking error converges to zero in 5 [s] under the

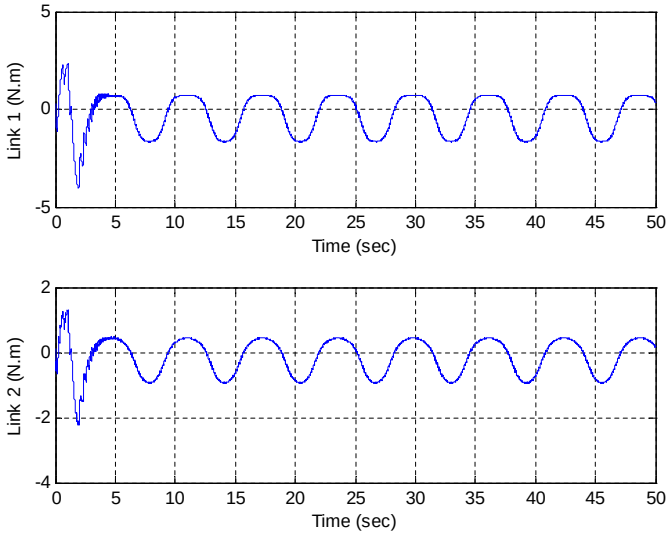

Figure 4.14: Control input signal.

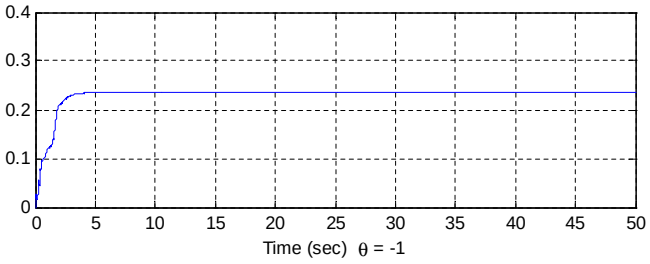

Figure 4.15: Parameter estimation result.

Table 4.3: Control Gains

Freestream velocity	K_{11}	K_{22}	Γ_{11}	Γ_{22}	κ
8 [m / s]	10	10	3	3	10
13.28 [m / s]	1	1	5	5	10

proposed control algorithm. The control signal is presented in Fig. 4.14 while the parameter estimation result is given in Fig. 4.15.

4.4.2 Application to Aeroelastic Model

Simulation results for a 2-D wing section model introduced in (4.75) and (4.76) under the proposed control also demonstrates the performance of the proposed controller. Note that in this simulation, the parameters in (4.75) and (4.76) are given in Table I. The parameters for the controller in pre- and post-flutter conditions are listed in Table 4.3.

while the adaptation gain are selected as $\Gamma_Y = 0.01$. When no external disturbance is considered, Fig. 4.16 shows the open-loop and closed-loop responses of wing section model at pre-flutter speed $U_\infty = 8$ [m / s]$< U_F = 11.4$ [m / s]. In Fig. 4.16(b), one can easily see that the proposed control law successfully drives the plunge and pitch displacements to zero within 2 [s]. Fig. 4.17(a) and Fig. 4.17(b) compare the open-loop and closed-loop responses of the system at post-flutter speed $U_\infty = 13.28$ [m / s]$> U_F = 11.4$ [m / s]; in the absence of any control input, LCOs are experienced due to the nonlinearities in the system model. The

control is turned on at $t = 5$ [s]. As one can see from Fig. 4.17(b), the pitching displacement converges to zero in less than 2 [s] while it takes a little longer time to suppress the plunging displacement oscillations.

Under a small sinusoid-like gust, with $w_0 = 0.047$ [m / s] at both pre-flutter speed and $w_0 = 0.07$ [m / s] at post-flutter speed, the closed-loop responses of the system are represented in Fig. 4.18. Compared with Fig. 4.16(b) and Fig 4.17(b), one can see that it takes nearly the same time (2 [s]) for the controller to suppress the pitching and plunging displacements even in the presence of a sustained external disturbance. One can also clearly see that the control signal is able to compensate for the sinusoidal disturbance injected into the wing section model.

The closed-loop responses of the system under a large triangular gust ($w_0 = 0.7$ [m / s]) are represented in Fig. 4.19 at both pre- and post-flutter speed. Note that this triangular gust is not $\mathcal{C}^2$ smooth and it can not be compensated all the time under current wing section model by a limited control signal. From Fig. 4.19(a), one can see that the proposed controller can suppress the pitching and plunging displacements in 4 [s] at pre-flutter speed. It's also clearly to see that it takes less than 3 [s] at post-flutter speed for the pitching and plunging displacements to converge to zero.

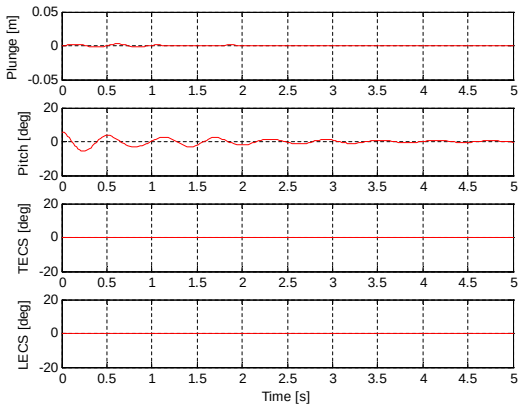

(a)

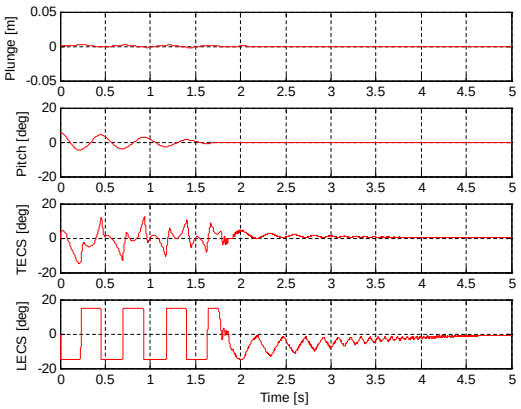

(b)

Figure 4.16: System response at pre-flutter speed $U_\infty = 8[m/s]$ (a): open-loop; (b): closed-loop.

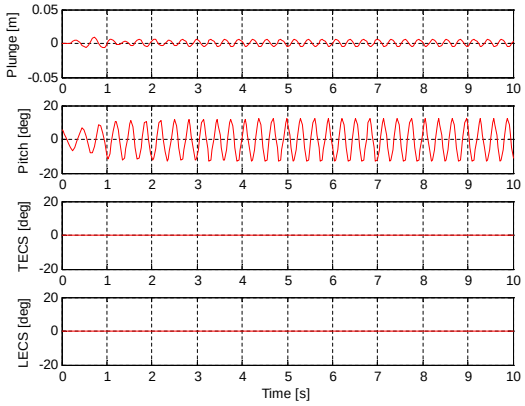

(a)

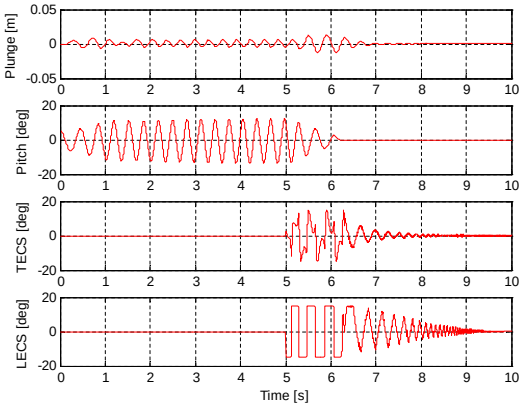

(b)

Figure 4.17: System response at post-flutter speed $U_\infty = 13.28[m/s]$ (a): open-loop; (b): closed-loop.

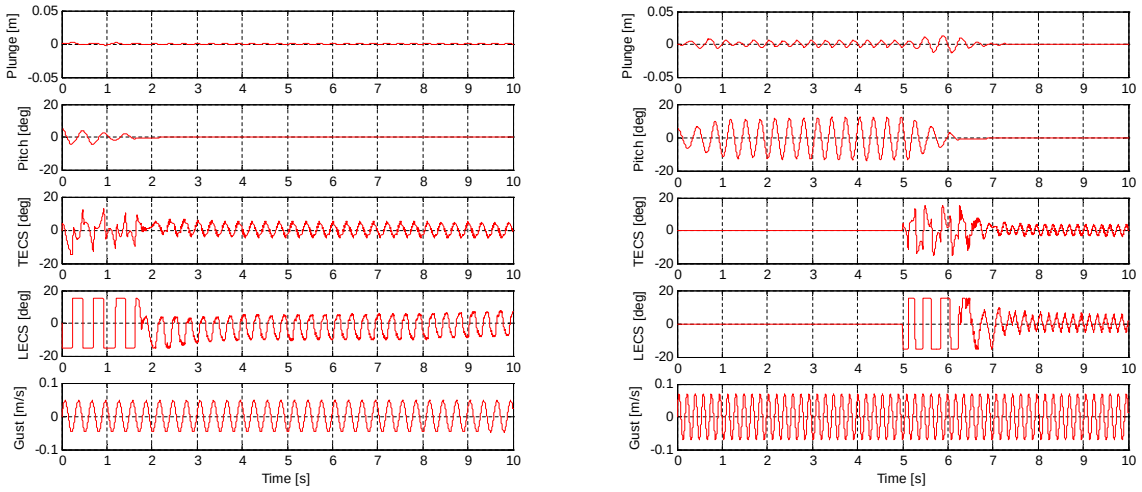

(a) (b)

Figure 4.18: System response under sinusoidal gust (a): at pre-flutter speed $U_\infty = 8[m/s]$; (b): at post-flutter speed $U_\infty = 13.28[m/s]$.

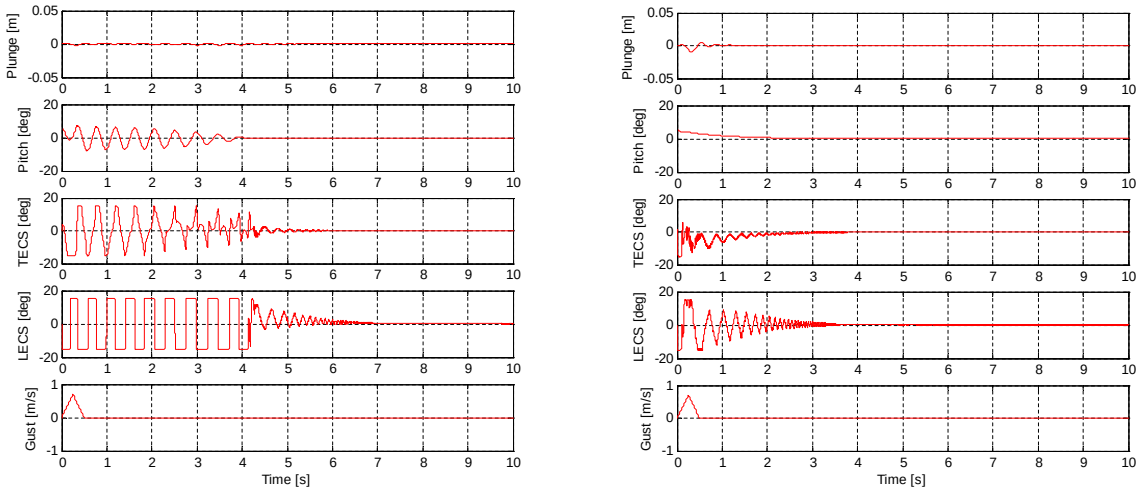

(a) (b)

Figure 4.19: System response under triangular gust (a): at pre-flutter speed $U_\infty = 8[m/s]$; (b): at post-flutter speed $U_\infty = 13.28[m/s]$.

CHAPTER 5

CONCLUSIONS

In this dissertation, we have documented the progress in Lyapunov-based design and engineering applications for a class of nonlinear MIMO systems. Four kinds of controllers, i.e., robust adaptive controller, adaptive output controller, model-free controller, and continuous robust controller have been proposed and verified through a 2-DOF robot manipulator model and 2- DOF aeroelastic model. Simulation results have demonstrated efficacy of the proposed control laws.

LIST OF REFERENCES

[1] A. S. Morse, "A Gain Matrix Decomposition and Some of Its Applications," *Syst. & Cont. Letters*, vol. 21, pp. 1-10, 1993.

[2] S. S. Sastry and M. Bodson, *Adaptive Control: Stability, Convergence, and Robustness*, Englewood Cliffs, NJ, Prentice-Hall, 1989.

[3] P. A. Ioannou and K. Sun, *Robust Adaptive Control*. Englewood Cliffs, NJ: Prentice-Hall, 1996.

[4] K. Narendra and A. Annaswamy, *Stable Adaptive Systems*, Englewood Cliffs, NJ, Prentice Hall, 1989.

[5] M. de Mathelin and M. Bodson, "Multivariable Model Reference Adaptive Control without Constraints on the High-Frequency Gain Matrix," *Automatica*, vol. 31, pp. 597-6045, 1995.

[6] S. R. Weller and G. C. Goodwin, "Hysteresis Switching Adaptive Control of Linear Multivariable Systems," *IEEE Trans. Aut. Cont.*, vol. 39, no. 7, pp. 1360-1375, 1994.

[7] R. R. Costa, L. Hsu, A. K. Imai, and P. V. Kokotović, "Lyapunov-Based Adaptive Control of MIMO Systems," *Automatica*, vol. 39, no. 7, pp. 1251-1257, 2003.

[8] L. Hsu, R. R. Costa, and F. Lizarralde, "Lyapunov/Passivity-Based Adaptive Control of Relative Degree Two MIMO Systems with an Application to Visual Servoing," *IEEE Trans. Aut. Cont.*, Minneapolis, vol. 52, no. 2, pp. 364-371, 2007.

[9] M. Krstić, I. Kanellakopoulos, and P. V. Kokotović, *Nonlinear and Adaptive Control Design*, John Wiley & Sons, 1995.

[10] G. Campion and G. Bastin, "Indirect Adaptive State Feedback Control of Linearly Parameterized Nonlinear Systems," *Int. Journal of Adaptive Cont. and Signal Processing*, vol. 4, pp. 345-358, 1990.

[11] I. Kanellakopoulos, P. V. Kokotović, and A. S. Morse , "Adaptive Output-Feedback Control of Systems with Output Nonlinearities," *IEEE Trans. Aut. Cont.*, vol. 37, no. 11, pp. 1666-1682, 1992.

[12] S. S. Sastry and A. Isidori, "Adaptive Control of Linearizable Systems," *IEEE Trans. Aut. Cont.*, vol. 34, no. 4, pp. 405-412, 1989.

[13] E. B. Kosmatopoulos and P. A. Ioannou, "Robust Switching Adaptive Control of Multi-Input Nonlinear Systems," *IEEE Trans. Aut. Cont.*, vol. 47, no. 4, pp. 610-624, 2002.

[14] H. Xu and P. A. Ioannou, "Robust Adaptive Control for a Class of MIMO Nonlinear Systems with Guaranteed Error Bounds," *IEEE Trans. Aut. Cont.*, vol. 48, no. 5, pp. 728-742, 2003.

[15] A. K. Imai, R. R. Costa, L. Hsu, G. Tao; P. V. Kokotović, "Multivariable adaptive control using high-frequency gain matrix factorization," *IEEE Trans. Aut. Cont.*, vol.49, no.7, pp. 1152- 1156, 2004.

[16] S. S. Ge and C. Wang, "Adaptive Neural Control of Uncertain MIMO Nonlinear Systems," *IEEE Trans. on Neural Networks*, vol. 15, no. 3, pp. 674-692, 2004.

[17] T. P. Zhang and S. S. Ge, "Adaptive neural control of MIMO nonlinear state time-varying delay systems with unknown dead-zones and gain signs," *Automatica*, vol. 43, pp. 1021-1033, 2007.

[18] Y. Wu and Y. Zhou. "Output Feedback Control for MIMO Non-linear Systems with Unknown Sign of the High Frequency Gain Matrix," *Int. Journal of Cont.*. vol 77, no. 1, pp. 9–18, 2004.

[19] X. T. Zhang, D. M. Dawson, M. S. de Queiroz, and B. Xian, "Adaptive Control for a Class of MIMO Nonlinear Systems with Non-Symmetric Input Matrix," in *Proc. of IEEE Conf. on Cont. Applications,* Taipei, Taiwan, pp. 1324-1329, 2004.

[20] J. Chen, A. Behal, and D. M. Dawson, "Adaptive Output Feedback Control for a Class of MIMO Nonlinear Systems," in *Proc. of the Amer. Cont. Conf.*, Minneapolis, MN, pp. 5300-5305, 2006.

[21] C. P. Bechlioulis, G. A. Rovithakis, "Robust Adaptive Control of Feedback Linearizable MIMO Nonlinear Systems with Prescribed Performance," *IEEE Trans. on Aut. Cont.*, vol. 53, pp. no. 9, 2090-2099, 2008.

[22] C. P. Bechlioulis, G. A. Rovithakis, "Prescribed Performance Adaptive Control for Multi-Input Multi-Output Affine in the Control Nonlinear Systems," *IEEE Trans. on Aut. Cont.*, vol. 55, no. 5, pp. 1220-1226, 2010.

[23] J. Back, H. Shim, "An Inner-Loop Controller Guaranteeing Robust Transient Performance for Uncertain MIMO Nonlinear Systems," *IEEE Trans. Aut. Cont.*, vol. 54, no. 7, pp.1601-1607, 2009.

[24] Y. Chang, "Block Backstepping Control of MIMO Systems", *IEEE Trans. Aut. Cont., accepted to be published.*

[25] P. Setlur, J. Wagner, D. M. Dawson, and J. Chen, "Nonlinear Controller for Automotive Thermal Management Systems," in *Proc. of Amer. Cont. Conf.*, Denver, CO, pp. 2584-2589, 2003.

[26] E. Zergeroglu, D. M. Dawson, M. S. de Queiroz, and A. Behal, "Vision-Based Nonlinear Tracking Controllers with Uncertain Robot-Camera Parameters," *IEEE/ASME Trans. Mechatronics*, 6, 322-337, 2001.

[27] K. Reddy, J. Chen, A. Behal, and P. Marzocca, "Multi-Input/Multi-Output Adaptive Output Feedback Control Design for Aeroelastic Vibration Suppression," *AIAA Jour. of Guid., Cont., and Dyn.*, vol. 30, no. 4, pp. 1040-1048, Jul-Aug 2007.

[28] Z. Wang, A. Behal, P. Marzocca, "Adaptive and Robust Aeroelastic Control of Nonlinear Lifting Surfaces with Single/Multiple Control Surfaces: A Review," *International Journal of Aeronautical and Space Sciences*, vol. 11, no. 2, pp. 69-79, 2010.

[29] Z. Wang, J. Chen, and A. Behal,"Robust Adaptive Control Design for a Class of Uncertain MIMO Nonlinear Systems," in *Proc. of IEEE Multi-Conference on Systems and Control-International Symposium on Intelligent Control (ISIC)*, Yokohama, Japan, Sep. 8-10, 2010, pp. 2284-2289.

[30] Z. Wang, A. Behal, P. Marzocca, "Model-Free Control Design for MIMO Aeroelastic System Subject to External Disturbance," *AIAA Jour. of Guid., Cont., and Dyn.*, vol. 34, no. 2, pp. 446-458, Mar./Apr. 2011.

[31] Z. Wang, A. Behal, B. Xian, and J. Chen, "Lyapunov-Based Adaptive Control Design for a Class of Uncertain MIMO NonlinearSystems," *2011 IEEE Multi-Conference on Systems and Control-International Symposium on Intelligent Control (ISIC),* submission under review.

[32] Z. Wang and A. Behal, "Continuous Robust Control for a Class of Uncertain MIMO Nonlinear Systems," *2011 IEEE Conference on Decision and Control,* submission under review.

[33] Z. Wang, A. Behal, P. Marzocca, "Continuous Robust Control for Plunging-Pitching Aeroelastic System with Leading- and Trailing-Edge Flaps," *AIAA Jour. of Guid., Cont., and Dyn.*, submission under review.

[34] B. Xian, M. S. de Queiroz, and D. M. Dawson, "A Continuous Control Mechanism for Uncertain Nonlinear Systems," in *Optimal Cont., Stabilization, and Nonsmooth Analysis*, 251-262, Heidelberg, Germany: Springer-Verlag., 2004.

[35] J. B. Pomet and L. Praly, "Adaptive Nonlinear Regulation: Estimation from the Lyapunov Equation," *IEEE Trans. Aut. Cont.*, vol. 37, no. 6, pp. 729-740, 1992.

[36] H. K. Khalil, "Adaptive Output Feedback Control of Nonlinear System Represented by Input-Output Models," *IEEE Trans. Aut. Cont.*, vol. 41, no. 2, pp. 177-188, 1996.

[37] H. Khalil, *Nonlinear Systems*, Prentice Hall, 1996.

[38] Z. Qu, *Robust Control of Nonlinear Uncertain Systems*, John Willey & Sons, Inc., 1998.

[39] A. N. Atassi and H. K. Khalil, "A Separation Principle for the Stabilization of a Class of Nonlinear Systems," *IEEE Trans. on Aut. Cont.*, vol. 44, no. 9, pp. 1672-1687, 1999.

[40] J. J. Slotine and W. Li, A*pplied Nonlinear Control,* New York, NY: Prentice Hall, 1991.

[41] A. P. Aguiar and J. P. Hespanha, "Position Tracking of Underactuated Vehicles," in *Proc. of Amer. Cont. Conf.*, Denver, CO, pp. 1988-1993, 2003.

[42] R. Marino and P. Tomei, "Global Adaptive Output-Feedback Control of Nonlinear Systems, Part I: Linear Parameterization ," *IEEE Trans. Aut. Cont.*, vol. 38, no. 1, pp. 17-32, 1993.

[43] P. Marzocca, L. Librescu, G. Chiocchia, "Aeroelastic Response of 2-D Lifting Surfaces to Gust and Arbitrary Explosive Loading Signatures," *International Journal of Impact Engineering*, vol. 25, pp. 41-65, 2001.

[44] K. K. Reddy, J. Chen, A. Behal, P. Marzocca, "Multi-Input/Multi-Output Adaptive Output Feedback Control Design for Aeroelastic Vibration Suppression," *AIAA Jour. of Guid., Cont., and Dyn.*, vol. 30, no. 4, 2007, pp. 1040-1048.

[45] F. L. Lewis, D. M. Dawson, and C. T. Abdallah, *Robot Manipulator Control: Theory and Practice,* CRC, 2rd edition, 2003.

[46] F. L. Lewis, C. T. Abdallah, and D. M. Dawson, *Control of Robot Manipulator*, New York: Macmillam, 1993.

[47] G. Platanitis and T. W. Strganac, "Control of a Nonlinear Wing Section Using Leading- and Trailing-Edge Surfaces," *AIAA Jour. of Guid., Cont., and Dyn.*, vol. 27, no. 1, 2004, pp. 52-58.

[48] K. J.Åström and L. Rundqwist, "Integrator Windup and How to Avoid It," in *Proc. Amer. Cont. Conf.*, Pittsburgh, PA, 1989, pp. 1693–1698.

[49] Z. Cai, M. S. de Queiroz, and D. M. Dawson, "A sufficiently smooth projection operator," *IEEE Trans. Aut. Cont.*, vol. 51, no. 1, pp. 135-139, 2006.